c1

A STUDY OF CIRCULAR COUETTE FLOW BY LASER DOPPLER MEASUREMENT TECHNIQUES

by

NIGEL D.S. GEACH

B.A. Sc., University of British Columbia, 1970

A THESIS SUBMITTED IN PARTIAL FULFILMENT OF

THE REQUIREMENTS FOR THE DEGREE OF

MASTER OF APPLIED SCIENCE

in the Department

of

Mechanical Engineering

We accept this thesis as conforming to the required standard

THE UNIVERSITY OF BRITISH COLUMBIA

FEBRUARY 1974

In presenting this thesis in partial fulfilment of the requirements for an advanced degree at the University of British Columbia, I agree that the Library shall make it freely available for reference and study. I further agree that permission for extensive copying of this thesis for scholarly purposes may be granted by the Head of my Department or by his representatives. It is understood that copying or publication of this thesis for financial gain shall not be allowed without my written permission.

Department of Mechanical Engineering

The University of British Columbia
Vancouver 8, Canada

Date April 16, 1974

ABSTRACT

A laser Doppler velocimeter is constructed and used to make flow measurements in circular Couette flow. The flow is created between concentric cylinders with a small gap-to-radius ratio, and measurements of the velocity profiles are made in both laminar and turbulent flow regimes. Distortion due to end effects is noted in the laminar case, but the turbulent case is shown to conform well to a three region model. A study of the mean velocity profiles allows estimates of skin friction and Reynolds stresses. Turbulent velocity fluctuations are also estimated from the laser Doppler technique, and their intensity compared with existing results for plane Couette flow.

TABLE OF CONTENTS

LIST OF FIGURES

NOMENCLATURE

A_τ	turbulent mixing coefficient
a,b	real and imaginary constants in the equation for Hamel spiral motion
b	distance to the midpoint of the flow
C_f	coefficient of friction
E	mean voltage output of LDV tracker
e'	fluctuating voltage output of LDV tracker
f, f_o, f_1	frequency components of LDV signal
H	curvilinear coordinate for spiral motion
h	2b, distance between inner and outer cylinder
K	conversion constant of optical geometry
ℓ	turbulence length scale, after von Karman
q_r, q_θ	radial and circumferential velocity components
R	Reynolds number based on cylinder velocity and gap width, $\frac{U_o h}{\nu}$
R_1	Reynolds number based on midstream velocity and half gap, $\frac{U_c b}{\nu}$ (R/4)
r_1, r_2	radii of inner and outer cylinders, respectively
S	core region slope, $\frac{b}{U_c} \frac{\partial U}{\partial y} \Big\|_{y=b}$
U	circumferential velocity of Couette flow
U_c	centerline flow velocity
U_o	outer cylinder velocity, $2U_c$
U ,u'	components of velocity normal to the clockwise rotated fringe pattern

u', v', w'	fluctuating velocity components of flow in Cartesian coordinates
u_*	friction velocity
u_i	velocity components in Navier-Stokes equations
V , v'	components of velocity normal to the clockwise rotated fringe pattern
$W(z)$	analytic function in Hamel's solution
x_i, x, y, z	Cartesian coordinate system
z	$x + iy$
α_1, α_2	constants of order unity in mixing length theory
ε	apparent or "eddy" viscosity
θ	half angle between the light beams
κ	von Karman constant, 0.4
λ	wavelength of light
μ	viscosity (absolute)
ν	viscosity (kinematic)
ρ	density
τ, τ_o	shear stress, shear stress at wall
τ_ℓ, τ_t	laminar and turbulent contributions to shearing stress
ϕ	curvilinear coordinate in Hamel spiral motion
ω	frequency of turbulent fluctuations
ω_1, ω_2	angular velocity of inner, outer cylinder respectively
ω_i	components of vorticity
ψ	stream function of flow

ACKNOWLEDGEMENTS

The author would like to thank Drs. I.S. Gartshore and E.G. Hauptmann for their advice and guidance in the course of this research.

The computing facilities of the Computing Centre of the University of British Columbia were used for the reduction of data contained herein.

This research was supported by the University of British Columbia and the National Research Council of Canada.

1. INTRODUCTION

Plane Couette flow is the simplest form of shear flow to treat mathematically, but is very difficult to create physically because of the difficulties involved in avoiding boundary effects. It is for this reason that rotating concentric cylinders with a small gap-to-radius ratio are often used to approximate the flow because of their physical simplicity. The shear flow between rotating concentric cylinders is also interesting in its own right because of the application to journal bearing design, or indeed any lubricated rotating system.

The number of workers who have made measurements in circular Couette flow since it was initially studied by Couette[1] [1870] is small. Some of the work includes the studies of Sir G.I. Taylor[2,3] [1923 and 1936] S.I. Pai[4] [1939], and D.C. McPhail [1941]. Further attempts have been made to measure plane Couette flow using immersed rod techniques by H. Reichardt[5] [1955], and with pitot tubes and hot wire anemometry by Robertson[6] [1959]. More recently the work of Coles and Van Atta[7] [1965] and of Coles[8] [1966] has produced information on spiral turbulence and accurate measurements of laminar circular Couette flow with end effects. Robertson and Johnson[9] [1970] have made measurements of the turbulence structure in plane Couette flow using conventional techniques.

With the advent of the laser, it became possible for the first time to employ optical techniques for flow velocity measurements, and this was demonstrated in 1964 by Yeh and Cummins[10] with their "laser-Doppler" velocimeter. This type of measuring technique lends itself to velocity measurement in circular Couette flow because the probe is simply an ellipsoid of light, with no potentially disturbing intrusions into the flow. For this reason, and because there are few known published measurements of turbulent circular Couette flow, it was decided a laser Doppler system should be developed and velocity measurements taken.

The system, which will be described in detail in a later chapter, essentially consists of two beams of laser light which cross. The small volume where they cross is the point of measurement with small particles which move with the fluid generating a frequency proportional to velocity. Typical laser Doppler signals are shown in Figure 1.1. The measurement of any mean velocity merely requires the ability to measure the mean frequency; while to measure a fluctuating velocity requires an ability to follow the changes in frequency.

In the report which follows is a description of circular Couette flow, both laminar and turbulent, and measurements which have been made in water contained in a circular Couette flow apparatus. Mean velocities have been measured, as well as some representative measurements of turbulence intensities and core region profile slopes.

2. THEORY

2.1 Laminar Couette Flow

The study of the laminar regime in circular Couette flow is of interest in that the theory is well developed and allows for accurate prediction of the velocity profiles of the flow between infinite cylinders. Laminar flow is also free of turbulent velocity fluctuations, so measurements can be made of the spectral or ambiguous broadening of the signal, an effect which will be discussed later in the text.

The ideal plane Couette flow profile is shown in Figure 2.1(a). This is created by an infinite upper plate moving with a velocity U_o with respect to an infinite stationary lower plate. The intervening fluid, which is incompressible, shears in such a way that the velocity at any height y is given by the relation:

$$U = \frac{U_o y}{h} \qquad 2.1$$

where h is the distance between plates. Furthermore, for laminar flow of a Newtonian fluid the shearing stress τ_ℓ is proportional to the slope of the velocity profile i.e.:

$$\tau_\ell = \mu \frac{dU}{dy} \qquad 2.2$$

This shearing stress increases rapidly upon transition from laminar to turbulent flow.

The exact profile of Couette flow between infinite concentric rotating cylinders can be predicted by solving the Navier-Stokes equations for incompressible flow (see Appendix I). The tangential velocity component is given by:

$$U = \frac{1}{r_2^2 - r_1^2}\left[r(\omega_2 r_2^2 - \omega_1 r_1^2) - \frac{r_1^2 r_2^2}{r}(\omega_2 - \omega_1)\right] \qquad 2.3$$

where r_1 and r_2 are the radii of the inner and outer cylinders respectively, which rotate with angular velocities ω_1 and ω_2. All measurements reported in this study have been made with the inner cylinder fixed, i.e., $\omega_1 = 0$, so that Equation 2.3 reduces to:

$$U = \frac{1}{r_2^2 - r_1^2}\left[r\omega_2 r_2^2 - \frac{r_1^2 r_2^2}{r}\omega_2\right] \qquad 2.4$$

Equation 2.4 is the basis of the theoretical curves plotted with measured laminar results.

2.2 Turbulent Couette Flow

Robertson [1959] has observed that his measurements of plane Couette flow in air line up well with Couette's concentric cylinder results. Thus, for the purposes of this study, the turbulent Couette flow between the cylinders is approximated by plane Couette flow because of the small gap to radius ratio of the apparatus (1:21). That the effect of curvature is minimal is borne out by the experimental profiles described in Chapter 4.

Turbulent plane Couette flow is approximated by three regions, as shown in Figure 2.1(b) after Reynolds[11] [1963]. These are the so-called "viscous sublayers" at either wall, a log-law region further from the wall, and a linear region in the core.

The viscous sublayers are assumed to have a Reynolds number so small that the Reynolds stresses are negligible, and that their thickness is of the order $10\nu/u_*$ [Tennekes and Lumley, 1972].[12] Furthermore, experimental evidence from pipe flow [Hinze, 1959][13] suggests the profile is more accurately approximated by assuming the eddy viscosity is nowhere larger than 0.07 bu_*.

The viscous sublayers are assumed to change abruptly to a log region, which extends well into the gap before merging into a linear region in the core. At the matching point, the core region velocity U and slope $\frac{\partial U}{\partial y}$ are equal to the velocity and slope of the log region. The composite velocity profiles have been worked out both with and without Hinze's restriction and can be found in Appendix II. These curves are plotted in conjunction with measured values, as described in Chapter 4.

The shearing stress τ remains constant across the gap (to a first approximation), and is equal to that at the wall (τ_o). This stress consists of the laminar contribution given by Equation 2.2 plus the turbulent contribution τ_t, where

$$\tau_t = A_\tau \left(\frac{\partial \bar{U}}{\partial y} \right) \qquad 2.5$$

with y measured from the stationary wall. The total shearing stress is then given by:

$$\tau = \tau_o = \tau_\ell + \tau_t = (\mu + A_\tau) \frac{\partial \bar{U}}{\partial y} \qquad 2.6$$

where A_τ is a mixing coefficient for the Reynolds stress in turbulent flow.

2.3 Reynolds Stresses

In addition to measurements of the mean velocity profiles, estimates of shear stresses are reported in Chapter 4. These shear stresses, or Reynolds stresses, arise from the interaction between the u' and v' components of the turbulence, as long as a shear layer exists, and can be demonstrated as the mechanism by which the wall stress is imparted to the opposite wall. For turbulent flow far from the wall, $\tau_t >> \tau_\ell$, hence

$$\tau = A_\tau \frac{\partial \bar{U}}{\partial y} = \rho\varepsilon \frac{\partial \bar{U}}{\partial y} \qquad 2.7$$

where ρ is density, and ε is eddy viscosity. From mixing length considerations, the following equalities are valid: (see reference 12)

$$\tau = -\rho \overline{u'v'} = \rho\varepsilon \frac{\partial \bar{U}}{\partial y} = \rho\ell^2 \left(\frac{\partial \bar{U}}{\partial y} \right)^2 \qquad 2.8$$

where $\overline{-u'v'}$ is a Reynold's stress, and ℓ is a mixing length.

Von Karman made the assumption that turbulent fluctuations are similar at all points in the field of flow. The mixing length ℓ can be chosen as the characteristic linear dimension for the fluctuation.

A friction velocity, u_*, which is characteristic of the turbulent motion, can be defined in terms of the shear stress as follows:

$$u_* = \sqrt{\frac{\tau}{\rho}} = \sqrt{|\overline{u'v'}|} \qquad 2.9$$

Thus τ also satisfies the following:

$$\tau = \rho u_*^2 = -\rho\, \overline{u'v'} \qquad 2.10$$

As seen from Appendix II, the value of u_* can be arrived at through the measurement of the velocity profiles. From these measurements, the Reynolds stress is estimated for turbulent circular Couette flow, and reported in Appendix VI.

3. INSTRUMENTATION

3.1 Background

The fact that the Doppler shift of laser light could be used to measure flow velocities was first demonstrated by Yeh and Cummins[10] [1964], and subsequent investigations by Goldstein and Kreid[14] [1967], Rudd[15] [1969], Durst and Whitelaw[16] [1970], and Greated[17] [1971] have all served to extend the technique. It is now commonly accepted that there are two separate and distinguishable modes of optical velocimeter operation, these being the reference beam technique (optical heterodyning) and the dual scatter mode (fringe pattern)(see Figures 3.1 and 3.2). The theory governing these different points of view is described in Appendix IV. The measurements performed during the course of the investigation reported herein were made with a dual-scatter system.

3.2 Components

Shown in Figure 3.3(a) is a block diagram of the dual scatter system used, while Figure 3.3(b) shows a photo of the experimental set-up. The beam source was a 15 milliwatt Spectra Physics Helium-Neon laser operating in the TEM-00 mode. The light wavelength was 6328 Angstroms and the beam diameter at point of splitting was 1.2 millimeters. The splitting was accomplished using a fifty percent beam splitter which gave two beams at an angle of 90 degrees. They were realigned parallel to within 0.1 percent using a front silvered mirror. Individual beam intensities measured between 5 and 6 milliwatts, indicating a certain amount of loss from the reflecting surfaces. The gap between the beams was measured as 11.68 millimeters.

An off-the-shelf 100 millimeter focal length lens was used to focus the light beams into a focal volume of approximately 0.07 millimeters in diameter and 0.64 millimeters in length. The resulting set of interference fringes was then imaged to the detecting surface of a Motorola PIN photodiode in an amplifying circuit by a 50 millimeter focal length PHYWE lens. The time varying signal frequency (whose mean covered a range of 2 to 200 Khz) was caused by foreward scattering of light from particles passing through the bright fringes at varying speeds. It was then band pass filtered to remove low and high frequency noise by a pair of Krohn-Hite model 3202 R filters before being fed into a DISA type 55L30 preamplifier. The DISA type 55L35 frequency tracker was then used to convert the frequency to a voltage, and this voltage was measured by DC and true RMS voltmeters (DISA type 55D30 and type 55D35 respectively). Visual monitoring of the signal was maintained throughout the experiments by a Tektronics model 502A dual-beam oscilloscope.

3.3 Calibration

The calibration of the DISA tracker was carried out as follows. In order to ascertain the accuracy of frequency to voltage conversion, a sinusoidal signal of known frequency was fed into the tracker unit from a signal generator, and the analogue output was measured by digital voltmeter. In all ranges tested, the tracker performed to manufacturer's specifications of 1 percent accuracy. Calibration curves appear in Figure 3.4(a). The AC capabilities of the DISA system were measured by triggering the signal generator with a second signal generator such that an artificial frequency modulation (slew rate) of the sinusoidal signal was created. The capture bandwidth, i.e. that region centred on the centre frequency (selected manually) was kept at its maximum of 8 percent, and the range of frequency fluctuations was varied up to 50 percent of the DC frequency. These curves appear in Figure 3.4(b). (See also Appendix V).

3.4 Signal Broadening

The signal being tracked is of the form

$$f = f_o \sin\omega t + f_1 \qquad 3.1$$

where f_1 is the DC component, f_o the range of fluctuation, and ω the frequency of fluctuation. Ideally if the probe volume were infinitely small and if the particles were in a continuous stream, the frequency f_1 would be given by the following:

$$f_1 = \frac{2U}{\lambda} \sin\theta \qquad 3.2$$

where U is velocity, λ is wavelength of the laser light, and θ the half angle of intersection. The frequency f_1 is directly proportional to the DC voltage from the frequency tracker. Similarly, with f_o the average amplitude of velocity fluctuations and ω their frequency (the majority less than 100 hz), the RMS voltage from the frequency tracker should be directly proportional to the RMS of the frequency f_o, hence also the velocity fluctuations $\sqrt{\overline{u'^2}}$. However, there exists in all optical anemometers an ambiguous broadening of the signal, which adds an uncertainty to any measured RMS values of voltage. Physically, this effect arises from the fact that θ is indeed a range of angles dependent on the beam diameter and lens focal length. An ideal representation of this broadening is obtained by differentiating Equation 3.2 with respect to θ, giving

$$\frac{df_1}{d\theta} = f_1 \operatorname{ctn} \theta \qquad 3.3$$

In practice, however, it is often more advisable to measure the broadening directly from a known laminar flow where fluctuations of velocity (hence frequency) do not exist. The broadening is then corrected for directly by subtraction of the mean square voltages from the turbulent and laminar contributions as follows:

$$\frac{\sqrt{\overline{u'^2}}}{U} = \left[\left(\frac{\Delta f}{f_1}\right)^2_{turb} - \left(\frac{\Delta f_\ell}{f_1}\right)^2_{lam}\right]^{1/2} \qquad 3.4$$

where Δf_ℓ is the measured broadening in laminar flow. (see Reference 19)

It must be noted that the use of Equation 3.4 as shown above represents a simplified approach to the problem of broadening. Generally in turbulent flow there exist the following effects: broadening due to variations in velocity across the scattering (probe) volume, Δf_T; and broadening due to the fluctuations of volume averaged velocity, Δfu_o.

Other factors which contribute to the broadening of the Doppler spectrum are gradients of mean velocity acroos the scattering volume Δf_G; Brownian motion of scattering particles, Δf_B; and the non-monochromaticity of the laser light source, Δf_S. Assuming these effects to be Gaussian, the bandwidth observed would be given as follows:

$$\Delta f^2 = \Delta f^2 u_o + \Delta f_T^2 + \Delta f_\ell^2 + \Delta f_G^2 + \Delta f_B^2 + \Delta f_S^2 \qquad 3.5$$

At present, nothing can be said of the contributions of the last three terms, except that they are small with respect to the first three. We are left with:

$$\Delta f^2 - \Delta f_\ell^2 = \Delta f^2{}_{u_o} + \Delta f_T^2 \qquad 3.6$$

The existence of Δf_T^2 is the factor which introduces the uncertainties into the turbulence measurements. For this reason, the results obtained using Equation 3.4 will be greater than the true values by an amount $\left(\frac{\Delta f_T}{f_1} \right)$. The justification for not attempting to compensate for this factor is that uncertainty of beam position (as described in the next section) is of the order of three percent. It also varies as the cylinder rotates because of its eccentricity, although refractive effects of the wall are negligible. The error introduced by Δf_T is small when compared with this effect.

Shown in Figure 3.5 is a calibration curve of the laminar broadening, which indicates a slight variation of the percentage with the output voltage of the tracker. Correction of turbulence measurements was carried out utilizing this curve, i.e., the value of ambiguous broadening was chosen depending on the mean D.C. voltage at the measuring point.

4. MEASUREMENTS AND RESULTS

4.1 The Flow Apparatus

The Couette flow under investigation was set up using water contained between two concentric plexiglas cylinders 24 inches in height and of radii 20.95 and 22.08 inches respectively (see Figure 4.1). The inner cylinder remained fixed at all times, the outer cylinder rotating at various speeds, governed by a VARIAC controlled 1 1/2 horse power electric motor which drove a reduction gear system, which in turn drove the cylinder via a belt drive. Due to the large inertia of the cylinder (wall plus base weighed over 100 lbs.), high frequency velocity fluctuations were eliminated. Long term drift in rotational speed was observed, but did not exceed 2 percent. Since measurements were made with the motor well warmed from running, drift was not expected to be a major factor.

4.2 Procedures

Early measurements consisted of traverses across the test section in order to get representative laminar and turbulent velocity profiles, while in later measurements turbulence intensities and Reynolds stresses were also attempted. The measurements were accomplished by mounting the optical components of the LDV on a moveable lathe bed. The large mass of the lathe bed reduced vibration to a minimum; and by moving the optics in the horizontal direction (normal to the cylinder walls) the beam intersection could traverse the gap. Displacement was measured to 0.001 inches by a micrometer fixed to the stationary part of the lathe bed. The receiving optics were mounted on a 0.5 meter optical bench, which in turn rested on a flat 0.5 inch thick base plate with rubber mat supports as vibration isolation.

Profiles were taken at varying heights above the base of the cylinders in an attempt to find a region of the flow which was relatively free from end effects. Unfortunately, since the height was of the same order as mean cylinder radius, end effects appeared in the laminar flow regime. Most traverses were made in the region between 2 and 4 inches below the free surface.

The water between the cylinders was seeded with small, approximately neutrally buoyant (density 1.05 gm/cc) polystyrene spheres of mean radius 0.372 microns in a concentration of about 1:100,000 by volume so as to increase the scattering of light to the detector. Drop-out (loss of signal) due to insufficient numbers of scattering centres was thus eliminated. However, refractive effects of the moving plexiglas caused the beams to misalign momentarily, placing an uncertainty on measurements which will be discussed later in the text.

Traverses were carried out in approximate steps of 0.05 inches, some to within 0.15 inches of the inner (stationary) cylinder wall. Closer proximity resulted in a D.C. flow frequency below the lower limit (2 Khz) of the DISA tracker, and therefore loss of tracking. The resulting profiles were then corrected for mean refractive effects on mean beam intersection position, normalized, and plotted.

In all, twenty-two traverses were carried out successfully, 7 in the laminar regime, 12 turbulent, and 2 in a regime which was assumed to be partially turbulent (transition). Flow visualization was attempted using dye. It was noted in the case of transition that the streaks exhibited laminar stability for much of the circumference, then rapidly broke into turbulent eddies and became well mixed. This phenomenon has been studied by Coles and van Atta [1966], and would lend itself readily to investigation by LDV methods.

In each traverse, care was taken to make readings at the same point on the outer cylinder circumference in order to minimize the slight effect of eccentricity, which was measured to be 3 percent of the gap width.

4.3 Analysis

The parameters measured were as follows: the position of the probe volume; the voltage (DC and true RMS) output of the frequency tracker; the mean frequency (as displayed on the tracker meter unit); and the percentage signal drop-out. The rotational speed of the outer cylinder was timed so as to give an independent measure of the mean velocity.

Throughout the experiments, it was discovered that the instantaneous mean velocity fluctuated up to 4 percent around the circumference. This was attributed to the eccentricity of the cylinder as previously mentioned, i.e. that the probe volume did not remain at a constant position in the flow. However, since measurements were taken on a damped voltmeter, and at the same circumferential position, this effect has been minimized.

4.4 Laminar Profiles

A total of seven laminar profiles were taken, at depths ranging from mid-height to within 0.5 inches of the free surface of the water. In all cases, consistent behavior was noted, with curvature markedly greater than predicted, probably as a result of end effects. This phenomenon has been noted by Coles [1966], in which laminar flow was maintained for Reynolds numbers up to 9,000. During the course of the present investigation, transition to turbulence was complete at Reynolds numbers of the order of 5,000. Comparison of two of the present results with those of Coles are shown in Figures 4.2 and 4.3. As well as mean velocity measurements, RMS voltages were also taken as a measure of the spectral broadening of the system. It was found that these values did not remain constant as expected, but appeared as a slight dependency on the mean voltage output of the tracker. Corrections to turbulent RMS voltages have been applied accordingly. Complete data from the laminar measurements are shown in Appendix VI.

4.5 Turbulent Profiles

Turbulent circular Couette flow as observed during the course of this study has exhibited reasonable agreement with the three-region theoretical model as described in Appendix II. The turbulent profile is highly dependent on the value of the friction velocity u_*, as well as assumptions made about the eddy viscosity ε. Appendix VI shows calculated parameters as a function of Reynolds number, while representative turbulent profiles are shown plotted in Figures 4.4 and 4.5. The measurements were made in the region between 2 and 4 inches below the free surface. Measurements were made successfully up to Reynolds numbers of the order of 16,000; beyond this point the tracker could not follow the flow due to distortion of the probe volume as a result of the rapidly rotating cylinder. Turbulent flow data is also contained in Appendix VI and a plot of core region slope against Reynolds number is shown in Figure 4.6.

4.6 Spectral Broadening

Since the analyzing equipment was readily available in the audio frequency range, measurements were made of the laminar flow spectrum in order to observe the ambiguous broadening of the LDV signal. Shown in Figure 4.7 is a typical spectrum which corresponds to a velocity of about 4.8 cm/sec at the 17 Khz peak. The existence of the secondary peak at 12 Khz is puzzling and unexpected, and it has been interpreted as a function of the moving plexiglas. Band pass filtering of the signal was used to reduce this effect, but this may still be a source of uncertainty in the calibration of the ambiguous (spectral) broadening.

4.7 Measurements of $\sqrt{\overline{u'^2}}$

Measurements of $\frac{\sqrt{\overline{u'^2}}}{U}$ were performed by correcting the measured RMS voltage for spectral broadening, then arriving at a percentage value by dividing by the mean DC voltage. Shown in Figure 4.8 are the values for Reynolds numbers of 6,256, 10,820, and 15,700. Robertson and Johnson [1970] report similar percentage values for measurements of u' in air. There appears to be a slight Reynolds number dependency evident from Figure 4.8, and this is contrary to the observations of Robertson and Johnson, which indicated that turbulence intensities were independent of flow Reynolds number.

4.8 Measurement of Reynolds Stresses

As described in Appendix III, the values of the Reynolds stress $\overline{u'v'}$ can be measured by taking the difference between the RMS voltages measured from each configuration (Figure 4.9). In order to simplify data reduction, the angle of fringe pattern rotation should be plus and minus 45°. Sample measurements of $\overline{u'w'}$ were made with the LDV probe volume directed normal to the cylinder wall. These results had large scatter, but were distributed about zero as expected due to the negligible shear in the z direction.

Attempts were then made to probe the flow from an angle different from the normal in an effort to get a component of $\overline{u'v'}$. These were unsuccessful due to the increased reflective loss of light intensity caused by an increased angle of incidence, combined with difficulties involved in the location of the light receiving optics.

4.9 Measurements of $\sqrt{\overline{w'^2}}$

As described in Appendix III, the slant fringe technique permits the measurement of the $\sqrt{\overline{w'^2}}$ component of turbulence. Representative values for the case of Re = 10820 are shown in Figure 4.10. It will be noted that these values are substantially smaller than the $\sqrt{\overline{u'^2}}/U$ values, and that they tend to approach zero further from the wall than the u' values. The large scatter encountered in measuring the rms voltages in the slant configurations make the accuracy of the w' measurements open to question, however it is probable that the indicated trend is accurate.

5. DISCUSSION

From the values obtained for mean flow velocities, it is seen that circular Couette flow in water is consistent and predictable. Using the mean profiles, and law-of-the-wall assumptions, it is possible to arrive at estimates of the friction coefficient C_f, the friction velocity u_*, and the shear stress τ. These values can then be compared with previous results and appropriate conclusions drawn.

Clauser[18] [1954] made extensive boundary layer measurements in a wind tunnel, and from these results was able to obtain a family of universal curves with C_f as a parameter. Experimental points taken near the wall are plotted, and C_f is determined by selecting the appropriate curve which fits the points. Shown in Figure 5.1 is the determination of C_f for the turbulent profiles reported, with U/U_c plotted against $\log_{10} \frac{yU_c}{\nu}$. As can be seen, allowing for scatter yields a friction coefficient in the order of 0.0035.

The previous results of Couette in water and Robertson in air showed a dependency of the C_f value on the Reynolds number given by the relation $0.072/(\log R_1)^2$. This relation is not apparent in the values reported in this study, although the values fall within a range shown in Figure 5.2, after Robertson and Johnson. It is felt that more accurate determination of C_f might result from torque measurements, rather than from log law inference as reported.

The friction velocity u_* is related to the shear stress τ by

$$u_* = \sqrt{\frac{\tau}{\rho}} \qquad 5.1$$

while the coefficient of friction C_f is

$$C_f = \frac{2\tau}{\rho U_c^2} \qquad 5.2$$

Thus u_* can be estimated directly from the C_f value by

$$u_* = U_c \sqrt{\frac{C_f}{2}} \qquad 5.3$$

Alternate values of u_* are arrived at by solving the equation for the velocity profile as given in Appendix II. Measured and calculated values of u_* appear in Appendix VI.

Further manipulation of the above relationships, combined with the core region slope $\frac{d\bar{U}}{dy}$ yields a measure of the eddy viscosity ε. From this the turbulent Reynolds number $\frac{U_c b}{\varepsilon}$ can also be found. This should remain approximately the same for the range of Reynolds numbers measured. The pertinent equations are as follows:

$$\frac{\tau}{\rho U_c^2} = \left(\frac{U_*}{U_c}\right)^2$$

$$= \frac{\varepsilon}{U_c^2}\frac{d\bar{U}}{dy} = \frac{\varepsilon}{U_c b}\frac{d\left(\frac{\bar{U}}{2U_c}\right)}{d\left(\frac{y}{2b}\right)} \qquad 5.4$$

The normalized core region slope S is given by

$$S = \frac{d\left(\frac{\bar{U}}{2U_c}\right)}{d\left(\frac{y}{2b}\right)} = \frac{b}{U_c}\frac{d\bar{U}}{dy} \qquad 5.5$$

so

$$\frac{U_c b}{\varepsilon} = \frac{S}{\left(\frac{u_*}{U_c}\right)^2} \qquad 5.6$$

These values also appear in Appendix VI, accompanied by some representative results from previous work.

As justification of log law relationships in the wall region, plots have been made of the normalized profiles on semi log paper, and the linear region becomes evident, as shown by the representative profile in Figure 5.3.

The RMS values of the turbulent velocity fluctuations in the circumferential (x) direction (i.e. $\sqrt{\overline{u'^2}}/U$) displayed a consistency in the core as expected, although the apparent slight Reynolds number dependency is surprising. The core region of the flow stays relatively constant in intensity, with a slight increase in the vicinity of the moving wall. This has been observed in previous work (Robertson and Johnson) as a more pronounced effect, and was also constrained to a thin layer closer to the wall. Of course, in the very near wall region, u' is expected to approach zero as a result of the dominant viscous effects, and this justifies the plot in Figure 4.8 being extended to the moving wall.

The most probable explanation for the rather broad region of increased turbulence intensity near the outer wall is that the wall is fluctuating some 3% of the gap width in position. This is due to the eccentricity effects cited earlier. Consequently, due to the fact that fairly long (up to 30 seconds) integration times were used in the RMS voltage measurements, a broad portion of the wall region has been sampled. The stationary wall region has the higher turbulence intensities, and had it been possible to make measurements in this region, the higher intensity would have been correspondingly more narrow because of the better spatial resolution. However, the low mean velocities in this region give rise to frequencies below the lower limit of the tracker, and thus measurement is impossible. One of Johnson's 1970 values for plane Couette flow in air has been included in Figure 4.8 as an indication of general agreement.

6. CONCLUSIONS

Laser Doppler velocimetry has been successfully used to make measurements of velocity profiles in both laminar and turbulent circular Couette flow. Physical limitations inherent in the apparatus have introduced an uncertainty to measured values close to the moving wall, while the natural limitations of laser Doppler systems have prevented measurements from being taken in the low velocity region close to the stationary wall. These limitations are the finite dimensions of the focal volume (0.64 mm in length) and the lower limit of velocity resolution (about 0.6 cm/sec). However, accurate measurement of core region slopes for varying Reynolds numbers has allowed the determination of the skin friction coefficient for the plexiglas cylinder, and subsequent estimates of shear stress and Reynolds stress. Furthermore, the complete turbulent profile across the gap has been shown to approximate a three region model as first proposed by Reynolds [1963] in studies of bearing turbulence, while laminar measurements have confirmed the existence of profile distortion, probably due to end effects, as observed by Coles.

Laser Doppler methods as applied to the measurement of turbulence intensities produced results which had somewhat greater scatter than those observed by conventional techniques in air. Also, turbulence intensities showed a slight Reynolds number dependency, which is contrary to findings in plane Couette flow in air. The air measurements were in a higher Reynolds number range, but further work is indicated in this area.

Estimates of the Reynold's stress $\overline{u'w'}$ in the core from slant fringe methods were found to exhibit scatter about zero as expected. The technique was also applied in an effort to measure $\overline{u'v'}$, the Reynold's stress which dominates because of the non-isotropy of the flow, but this was unsuccessful for reasons discussed in the text.

The w' component of turbulence reported is lower than the u' component, and does not exhibit an increase near the moving wall. Its measurement comes about from the slant measurements, and is subject to large scatter. Due to the small number of points, no conclusions can be drawn other than that the intensity is low.

It is felt that LDV methods can be significant in taking measurements in difficult situations. Further work in Couette flows is feasible; of special interest would be the transition regime. The obvious advantages of the LDV system, i.e. the absence of flow-disturbing probes combined with a linear response, make it the most practical tool available for this type of measurement. The versatility of the system will make it the logical choice for many future applications.

The significance of this work has been to provide measurements of circular Couette flow which have not been affected by the presence of a probe. Whether or not a probe does produce a substantial disturbing effect in measurements of such a flow has not been investigated in this study, but the possibility has been removed by the use of the LDV technique.

REFERENCES

1. Couette, M. "Etudes sur le frottement des liquids," Ann. de Chemie et de Physique, Ser. 6, Vol. 21, 1890, pp. 433-510.

2. Taylor, G.I. "Stability of a viscous liquid contained between two rotating cylinders," Phil. Trans. 1923, A 223, 289.

3. Taylor, G.I. "Fluid Friction Between Rotating Cylinders," Proc. Roy. Soc., A 157, pp. 546-564.

4. Pai, S.I. "Turbulent Flow Between Rotating Cylinders," NACA TN 892, March 1943.

5. Reichardt, H. "Uber die geschwindigkeitsverteilung in einer geradlinigen turbulenten Couette strömung," ZAMM Sonderheft, Vol. 36, 1956, pp. S26-29.

6. Robertson, J.M. "On Turbulent Plane Couette Flow," Proceedings of the Sixth Midwest Conference on Fluid Mechanics, 1959, pp. 169-182.

7. Van Atta, C., "Exploratory measurements in spiral turbulence," J. Fluid Mech. (1966), Vol. 25, Part 3, pp. 495-512.

8. Coles, D; and Van Atta, C. "Measured distortion of a laminar circular Couette flow by end effects," J. Fluid Mech. (1966), Vol. 25, Part 3, pp. 513-521.

9. Robertson, J.M., and Johnson, H.F. "Turbulence Structure in Plane Couette Flow," Journal of the Engineering Mechanics Division, ASCE, Vol. 96, No. EM6, Proc. Paper 7754, Dec. 1970, pp. 1171-1182.

10. Yeh, H., and Cummins, H.Z., "Localized fluid flow measurements with He-Ne laser spectrometer," Appl. Phys. Lett. 4, 176, 1964.

11. Reynolds, A.J. "Analysis of Turbulent Bearing Films." Journal Mechanical Engineering Science, Vol. 5, No. 3, 1963, pp. 258-272.

12. Tennekes, H., and Lumley, J.L. "A First Course in Turbulence." The MIT Press, 1972.

13. Hinze, J.O. "Turbulence, An Introduction to Its Mechanism and Theory." McGraw-Hill, 1959.

14. Goldstein, R.J., and Kreid, D.K. "Measurement of Laminar Flow Development in a Square Duct using a Laser-Doppler Flowmeter." Journal of Applied Mechanics, E, Vol. 34, pp. 813-818, 1967.

15. Rudd, M.J. "A New Theoretical Model for the Laser Dopplermeter." J. Sci. Instruments, 2, pp. 55-58, 1969.

16. Durst, F., and Whitelaw, J.H. "Optimization of Optical Anemometers." Imperial College, Mech. Eng. Dept., ET/TN/A/1.

17. Greated, C.A. "Resolution and back scattering optical geometry of laser Doppler systems." Journal of Physics E: Scientific Instruments, Vol. 4, pp. 585-588, 1971.

18. Clauser, F.H. "Turbulent Boundary Layers in Adverse Pressure Gradients." Journal of the Aeronautical Sciences, Feb. 1954, pp. 91-108.

19. George, W.K., and Lumley, J.L. "The laser-Doppler velocimeter and its application to the measurement of turbulence." J. Fluid Mech. (1973), Vol. 60, Part 2, pp. 321-363.

APPENDIX I

EXACT SOLUTION OF THE NAVIER-STOKES EQUATIONS FOR LAMINAR CIRCULAR COUETTE FLOW

We have:

$$\frac{\partial u_i}{\partial t} + u_k \frac{\partial u_i}{\partial x_k} = - \frac{1}{\rho} \frac{\partial p}{\partial x_i} + \nu \frac{\partial^2 u_i}{\partial x_k^2} \qquad 1$$

$$\frac{\partial u_k}{\partial x_k} = 0$$

Since the flow is parallel,

$$u_1 = u_1(x_2, t) \qquad 2$$

$$u_2 = u_3 = 0$$

Defining vorticity, i.e.:

$$\omega_j = \frac{\partial u_i}{\partial x_k} - \frac{\partial u_k}{\partial x_i} \qquad 3$$

leads to the vorticity equation:

$$\frac{D\omega_j}{Dt} - \omega_k \frac{\partial u_j}{\partial x_k} = \frac{\partial \omega_j}{\partial t} + u_k \frac{\partial \omega_j}{\partial x_k} - \omega_k \frac{\partial u_j}{\partial x_k} = \nu \frac{\partial^2 \omega_j}{\partial x^2_k} \qquad 4$$

The first term on the left represents total variation of vorticity with time, while the second term represents deformation of a vortex tube. The right represents diffusion of vorticity due to viscosity.

In two dimensional flow, deformation terms vanish, and 4 becomes:

$$\frac{\partial \omega}{\partial t} + u_k \frac{\partial \omega}{\partial x_k} = \nu \frac{\partial^2 \omega}{\partial x_k^2} \qquad k = 1,2 \qquad 5$$

Introducing the stream function ψ, where

$$\frac{\partial \psi}{\partial x_2} = u_1 , \qquad \frac{\partial \psi}{\partial x_1} = - u_2 \qquad 6$$

and

$$\omega = - \left(\frac{\partial^2 \psi}{\partial x_1^2} + \frac{\partial^2 \psi}{\partial x_2^2} \right) = - \Delta\psi \qquad 7$$

gives

$$\frac{\partial \Delta\psi}{\partial t} + \frac{\partial \psi}{\partial x_2} \frac{\partial \Delta\psi}{\partial x_1} - \frac{\partial \psi}{\partial x_1} \frac{\partial \Delta\psi}{\partial x_2} = \nu\Delta\Delta\psi \qquad 8$$

This is the vorticity transport equation. In steady flow (no time variation) this becomes:

$$\frac{\partial \psi}{\partial x_2} \frac{\partial \Delta\psi}{\partial x_1} - \frac{\partial \psi}{\partial x_1} \frac{\partial \Delta\psi}{\partial x_2} = \nu\Delta\Delta\psi \qquad 9$$

Hamel found solutions of 9 such that

$$\psi = f(\phi) , \quad \begin{array}{l} \Delta \phi = 0 \\ \Delta \psi \neq 0 \end{array}$$

Introducing an analytic function $W(Z) = W(x_1 + i x_2)$ such that

$$W(z) = \phi + iH \qquad 10$$

Hamel found that if the analytic function W satisfied the following condition,

$$2 \frac{d^2W/dz^2}{(dW/dz)^2} = a + ib = \text{const.} \qquad 11$$

the function $f(\phi)$ satisfies the following:

$$f'' f'b = \nu[f^{iv} + f'' (a^2+b^2)+ 2f'''a] \qquad 12$$

(primes refer to differentiation w.r.t. ϕ)

Integration of 11 gives

$$\phi = \frac{2}{a^2+b^2} (a \log r + b \theta) + \phi_0 . \qquad 13$$

where ϕ_0 is a constant of integration, and the polar coordinates r and θ are defined by

$$z - z_0 = re^{i\theta} \quad \text{with} \quad z_0 = \text{const.} \qquad 14$$

The streamline ϕ = constant is a logarithmic spiral,

i.e. $a \log r + b\,\theta$ = constant. When $b = 0$, the streamlines are concentric circles r = constant.

The velocity components are:

$$q_r = \frac{-ab}{a_2+b^2}\,\frac{f'}{r} \qquad 15$$

$$q_\theta = \frac{2a}{a^2+b^2}\,\frac{f'}{r} \qquad 16$$

For $b = 0$, Equation 12 gives

$$f' = C + r^2\,(A + B \log r) \qquad 17$$

with

$$q_r = 0\ , \quad q_\theta = \frac{2}{a}\left(\frac{C}{r} + Ar + Br \log r\right) \qquad 18$$

For the case of two concentric rotating cylinders, constant B must be zero because the pressures at $\theta = \theta$ and $\theta = \theta + 2\pi$ are the same. Thus,

$$q_\theta = \frac{2}{a}\left[\frac{C}{r} + Ar\right]\ , \quad q_r = 0 \qquad 19$$

Applying appropriate boundary conditions leads to the velocity components as stated in the text.

Since the gap is small with respect to the radius, we may let $r = r_1 + \Delta$, where r_1 is the inner cylinder radius, Δ is variable, and $\frac{\Delta}{r_1} << 1$ everywhere.

Then,

$$q_\theta = \frac{C_1}{r} + C_2 r$$

$$= \frac{C_1}{r_1(1+\frac{\Delta}{r_1})} + C_2(r_1+\Delta) \qquad 20$$

Expanding by the binomial theorem gives

$$q_\theta \simeq C_2 r_1 + \frac{C_1}{r_1} + C_2\Delta + C_1 \left(\frac{\Delta}{r_1^{\,2}}\right)$$

$$= A' + B'\Delta \qquad 21$$

where $A' = C_2 r_1 + \frac{C_1}{r_1}, \quad B' = C_2 + \frac{C_1}{r_1^{\,2}}$

Since $q_\theta = 0$ when $\Delta = 0$, $A' = 0$, and $q_\theta \simeq B'\Delta = B'(r-r_1)$. So to a first approximation, q_θ is a linear distribution, as in the plane case. This result indicates that the small gap-to-radius ratio justified the use of a plane model in the turbulent flow.

APPENDIX II

A THREE REGION MODEL FOR TURBULENT COUETTE FLOW

(a) No modification

Starting from the a priori assumption of $\frac{yu_*}{\nu} \leq 10$ (i.e. that the viscous sublayer thickness is $\frac{10\nu}{u_*}$) the velocity can be matched to the log law in the wall layer.

Region 1. Viscous sublayer:

$$\tau = \tau_o = \rho u_*^2 = \mu \frac{\partial U}{\partial y} \qquad 1$$

Integrating gives:

$$U = \frac{u_*^2 y}{\nu} \qquad 2$$

Region 2. Log law region

$$\frac{\partial U}{\partial y} = \frac{u_*}{\kappa y} \qquad 3$$

where κ is von Karman's constant.

Integrating gives:

$$\frac{U}{u_*} = \frac{1}{\kappa} \log y + C_1 \qquad 4$$

Matching velocities at $y = \frac{10\nu}{u_*}$ gives C_1, and 4 becomes:

$$\frac{U}{u_*} = \frac{1}{\kappa} \log \left(\frac{u_* y}{\nu}\right) - \frac{1}{\kappa} \log 10 + 10 \qquad 5$$

Region 3. Linear Region

From the scale relation between vorticity of the turbulence and vorticity of the mean flow, we have

$$\frac{u_*}{\ell} = \alpha_1 \frac{\partial U}{\partial y} \qquad 6$$

where α_1 is a coefficient of order 1 and ℓ is a length scale of the turbulence. Assuming $\ell \propto b$ in the core, 6 above integrates to

$$\frac{U}{u_*} = \frac{y}{\alpha_1 b} + C_2 \qquad 7$$

We know $U = U_c$ at $y = b$, thus:

$$\frac{U}{u_*} = \frac{y}{\alpha_1 b} + \frac{U_c}{u_*} - \frac{1}{\alpha_1} \qquad 8$$

Matching derivatives between log and linear regions at $y = y_m$:

$$\left.\frac{\partial U}{\partial y}\right|_{y=y_m} = \frac{u_*}{b\alpha_1} = \frac{u_*}{\kappa y_m}, \quad \text{so } b\alpha_1 = \kappa y$$

$$\text{and} \quad y_m = \frac{b\alpha_1}{\kappa}$$

Matching the velocities at y_m, we obtain a relationship between $\frac{U_c}{u_*}$ and α_1, as follows:

$$\left.\frac{U}{u_*}\right|_{y=y_m} = \frac{1}{\kappa} + \frac{U_c}{u_*} - \frac{1}{\alpha_1} = \frac{1}{\kappa}\log\left(\frac{b\alpha_1}{\kappa}\frac{u_*}{\nu}\right) - \frac{1}{\kappa}\log 10 + 10 \qquad 9$$

$$\text{or} \quad \kappa\frac{U_c}{u_*} + \log\frac{U_c}{u_*} = \log\left(\frac{bU_c}{\nu}\right) + \log\left(\frac{bU_c}{\nu}\right) + \log\left(\frac{\alpha_1}{10\kappa}\right) + (10\kappa - 1) + \frac{\kappa}{\alpha_1}$$

For any given Reynolds number $(\frac{bU_c}{\nu})$ this equation relates α_1 to $(\frac{U_c}{u_*})$. If α_1 is chosen by means of a best fit to a measured profile, $\frac{U_c}{u_*}$ can be estimated from this equation; alternatively, if $\frac{U_c}{u_*}$ is found using a best fit to the log law region (Clauser technique) then α_1 can be estimated using this equation (all profiles showed an α_1 in the range of 0.05 to 0.1). In either case, the equation above assumes a known viscous sublayer thickness, which is built into the derivation above.

(b) The Three Region Model with Hinze's Modification

In the three region model, the effective kinematic viscosity ($\varepsilon = \tau/\rho\frac{\partial U}{\partial y}$) is constant in the core region and varies linearly in the log region, since τ is constant to a first approximation. Thus, ε reaches a maximum in the core region, and if this value is given by $\varepsilon \leq 0.07\ bu_*$, then the value of α_1 is equal to 0.07, i.e.:

$$\varepsilon = 0.07\ bu_* = \frac{\rho u_*^2}{\rho\frac{\partial U}{\partial y}} \qquad 10$$

from the definition of ε, and the fact that $\tau = \rho u_*^2$ = constant. However, $\frac{\partial U}{\partial y} = \frac{u_*}{b} \frac{1}{\alpha_1}$ in the core, so that

$$0.07\ bu_* = \frac{u_*^2}{\frac{u_*}{b} \frac{1}{\alpha_1}}, \quad \text{or} \quad \alpha_1 = 0.07 \quad . \qquad 11$$

If ε reaches a maximum less than .07 u_* in the core region, then the previous model, described in (a) is applicable.

Using α_1 = .07, and Equation 9 the value of $\frac{u_*}{U_c}$ can be found, for any $(\frac{U_c b}{\nu})$ within the assumptions of the three region model with the assumed viscous sublayer thickness. The friction coefficient $(C_f = 2(\frac{u_*}{U_c})^2)$ can be found as a function of $\frac{U_c b}{\nu}$ within Hinze's assumption and is plotted in Figure 5.2 for comparison with other data.

APPENDIX III

MEASUREMENTS OF REYNOLDS STRESSES BY LASER DOPPLER VELOCIMETRY

Consider the simplistic approach as shown schematically in Figure 4.9. We have measured voltages which are directly related to velocity by a constant K, both mean and fluctuating thus:

$$KE = U_\perp = \frac{\bar{U}}{\sqrt{2}}$$

1

$$Ke' = u'_\perp$$

For the two configurations shown, we have the following equations:

$$U_\perp + u'_\perp = \frac{1}{\sqrt{2}} (\bar{U} + u' + w') \quad 2$$

$$V_\perp + v'_\perp = \frac{1}{\sqrt{2}} (\bar{U} + u' - w') \quad 3$$

Taking root mean squares of Equation 2 yields the following:

$$(U_\perp + u'_\perp)^2 = U_\perp^2 + 2U_\perp u_\perp' + u_\perp'^2$$

$$= K^2 (E_1^2 + 2E_1 e_1' + e_1'^2)$$

$$\sqrt{\overline{(U_\perp + u_\perp'}} = K\bar{E}_1 (1 + \frac{1}{2} \frac{\overline{e_1'^2}}{E_1^2} + \text{higher order terms}) \quad 4$$

Operating now on the right hand side of Equation 3 yields:

$$\frac{1}{2}(\bar{U}+u'+w')^2 = \frac{1}{2}(\bar{U}^2+u'^2+w'^2+2U(u'+w')+ 2u'w')$$

$$\frac{1}{\sqrt{2}} \sqrt{\overline{(\bar{U}+u'+w')^2}} = \frac{\bar{U}}{\sqrt{2}} (1 + \frac{1}{2} \frac{\overline{u'^2}}{\bar{U}^2} + \frac{1}{2} \frac{\overline{w'^2}}{\bar{U}^2} + \frac{\overline{u'w'}}{\bar{U}^2}$$

$$+ \text{ higher order terms}) \qquad 5$$

Similarly Equation 3 yields

$$\sqrt{\overline{(V_\perp + v_\perp')^2}} = K\bar{E}_2 (1 + \frac{1}{2} \frac{\overline{e_2'^2}}{\bar{E}_2^2} + \text{ higher order terms}) \qquad 6$$

and

$$\frac{1}{\sqrt{2}} \sqrt{\overline{(\bar{U} + u'-w')^2}} = \frac{U}{\sqrt{2}} (1+ \frac{1}{2} \frac{\overline{u'^2}}{\bar{U}^2} + \frac{1}{2} \frac{\overline{w'^2}}{\bar{U}^2} - \frac{\overline{u'w'}}{\bar{U}^2}$$

$$+ \text{ higher order terms}) \qquad 7$$

Subtracting Equations 6 and 7 from Equations 4 and 5 results in

$$\overline{u'w'} = \frac{\sqrt{2}}{4} \frac{\bar{U}K}{\bar{E}} (\overline{e_1'^2} - \overline{e_2'^2}) \qquad 8$$

where $\bar{E} = \bar{E}_1 = \bar{E}_2$. Recalling Equation 1, this simplifies to

$$\overline{u'w'} = \frac{K^2}{2} (\overline{e_1'^2} - \overline{e_2'^2}) \qquad 9$$

where K is the calibration constant which is a function of the laser Doppler system.

By adding equations 5 and 7, and equating their sum to the sum of Equations 6 and 8, the following expression arises:

$$\frac{\overline{u'^2}}{\bar{U}^2} + \frac{\overline{w'^2}}{\bar{U}^2} = \frac{\frac{1}{2}\,\overline{e_1'^2} + \frac{1}{2}\,\overline{e_2'^2}}{\bar{E}^2}$$

If a value of $\frac{u'^2}{\bar{U}^2}$ is known, then estimates of the w' component of turbulence can be found.

APPENDIX IV

THEORETICAL DESCRIPTION OF THE LASER DOPPLER VELOCIMETER

(a) Reference Beam Operation

Figure 3.1 shows geometrically the Doppler shift of laser light incident on a particle moving in a fluid. The number of wavefronts incident on the particle per unit time is:

$$\nu_p = \left(\frac{c - \vec{v}\cdot\hat{k}_i}{\lambda_i}\right) \qquad 1$$

After scattering, an observer in the direction $\hat{k}_{sc}$ would observe an apparent wavelength of:

$$\lambda_{sc} = \left(\frac{c - \vec{v}\cdot\hat{k}_{sc}}{\nu_p}\right) = \lambda_i\left(\frac{c - \vec{v}\cdot\hat{k}_{sc}}{c - \vec{v}\cdot\hat{k}_i}\right) \qquad 2$$

The frequency of this scattered radiation is given by:

$$\nu_{sc} = \frac{c}{\lambda_i}\left(\frac{c - \vec{v}\cdot\hat{k}_i}{c - \vec{v}\cdot\hat{k}_{sc}}\right) = \frac{c}{\lambda_i}\left[\frac{1 - \frac{\vec{v}\cdot\hat{k}_i}{c}}{1 - \frac{\vec{v}\cdot\hat{k}_{sc}}{c}}\right] \qquad 3$$

and the frequency shift is given by:

$$\nu_o = \nu_{sc} - \nu_i = \frac{c}{\lambda_i}\left[\frac{1 - \frac{\vec{v}\cdot\hat{k}_i}{c}}{1 - \frac{\vec{v}\cdot\hat{k}_{sc}}{c}}\right] - \nu_i$$

$$= \frac{1}{\lambda_i} \left[\frac{\vec{v}\cdot(\hat{k}_{sc} - \hat{k}_i)}{1 - \frac{\vec{v}\cdot\hat{k}_{sc}}{c}} \right]$$

$$\simeq \frac{1}{\lambda_i} \left[\vec{v}\cdot(\hat{k}_{sc} - \hat{k}_i) \right] \qquad 4$$

This frequency difference can be measured when the scattered light is heterodyned with an unscattered reference beam on the face of a square law optical detector such as a photomultiplier tube or a photodiode.

(b) Dual Scatter Operation

The dual scatter system requires the formation of a focal volume containing a fringe pattern, as shown in Figure 3.2. This is accomplished by the intersection of two equal intensity laser light beams which set up fringes of known geometry. If the angle between the beams is 2θ, the fringe spacing is given by

$$d = \frac{\lambda_i}{2 \sin \theta}$$

where both λ_i and θ are measured in the fluid.

As the scattering centre traverses the focal volume (interference pattern) with a velocity v, light is emitted with a frequency which corresponds to the rate at which the bright fringes are cut. This frequency is given by:

$$\nu = \frac{v}{d} = \frac{2v}{\lambda_i} \sin\theta \qquad 6$$

Equation 4 in (a) reduces to Equation 6 above if the angle between incident and reference beams is 2θ. The two different governing principles result in identical equations for velocity.

APPENDIX V

Tracker Calibration

(a) Frequency Tracking

The DISA type 55L35 frequency tracker was used to process the laser Doppler signal from the flow. Although the instruction manual presented data on the tracking performance of the unit, an independent study was also undertaken.

Initially, a pure sine wave input was fed to the tracker, which was tested in each range. The frequency to voltage conversion was within one percent for all ranges used, i.e. 15, 50, 150, and 500 khz. The curves normalized to produce the composite shown in Figure 3.4(a).

As an independent test on the rate at which the tracker would follow frequency fluctuations, one signal generator was connected so as to vary the frequency of a second signal generator. This produced a signal of the form

$$f = f_1 + f_0 \sin \omega t$$

where ω was the rate at which the frequency was varied. Various amplitudes of fluctuation about the mean frequency f_1 were tested, resulting in the curves shown in Figure 3.4(b). Since the ratio of frequency fluctuation to mean frequency seldom exceeded 10 percent, it can be seen that the tracker was consistently following fluctuations of 200 hz and below, and often following fluctuations up to 1000 hz.

(b) Ambiguous Broadening

Measurements of the RMS voltage output of the frequency tracker taken in laminar flow produced a spectral broadening in the order of 3 percent. However, this value had a slight dependence on the mean DC voltage output of the tracker, and is shown graphically in Figure 3.5. This effect was felt to be a function of the tracker rather than a physical effect in the flow, because theory predicts that the broadening is a function of the optics alone. Figure 3.5 results from measurements made in the 15 and 50 Khz ranges, and corrections for the 150 Khz range have been assumed to be the same, as there is no reason to suspect otherwise. Since 150 Khz corresponds to a velocity of over 40 cm/sec, flow in this range was turbulent and thus it could not be checked for inconsistancies. Corrections were applied to the RMS voltage by subtracting the ambiguous value which corresponded to the voltage produced by the mean velocity, as per Figure 3.5. Thus turbulence levels have been corrected for the slight non-linearity of the tracker.

APPENDIX IV

CALCULATED FLOW PARAMETERS

R	$U_c \frac{cm}{sec}$	S	$u_* \frac{cm}{sec}$	ε	$\frac{bU_c}{\varepsilon}$	C_f
5186	9.04	.543	.39 - .43	.045 - .054	291,239	0.0035
5338	9.30	.432	.39 - .41	.054 - .060	245,222	0.0034
6027	10.50	.461	.44 - .47	.057 - .065	262,230	0.0030
6055	10.55	.462	.44 - .47	.057 - .065	265,233	0.0035
6200	10.80	.519	.45 - .49	.056 - .062	298,252	0.0030
10,820	18.85	.425	.79 - .80	.112 - .115	242,236	0.0035
13,800[1]	24.04	.360	1.1	.19	181	-
15,700	27.35	.393	1.14 - 1.13	1.74	226	0.0035
18,400[2]	-	.240	-	-	-	0.0054
23,200[2]	-	.195	-	-	-	0.0052
27,000[2]	-	.217	-	-	-	0.0048

[1]Murguly (1971, unpublished).

[2]Robertson (1959).

$LIST PROFIL

R=1020 OUTER CYLINDER VELOCITY = 3.56 CM/SEC

POSIN(IN)	DC VOLTS	THETA	FREQUENCY	POSIN(MM)	VELOCITY(MM/SEC)
1.0000	8.7000	0.0874	13.0500	0.0048	35.5771
0.9816	8.6300	0.0874	12.9450	0.6187	35.2813
0.9426	8.3000	0.0874	12.4500	1.9196	33.9130
0.8971	8.0400	0.0875	12.0600	3.4348	32.8289
0.8578	7.7900	0.0876	11.6850	4.7472	31.7899
0.8030	7.4000	0.0876	11.1000	6.5625	30.1743
0.7646	7.0700	0.0877	10.6050	7.8361	28.8127
0.7280	6.9000	0.0877	10.3500	9.0489	28.1049
0.6878	6.6000	0.0878	9.9000	10.3796	26.8673
0.6556	6.3600	0.0878	9.5400	11.4443	25.8782
0.6242	6.0600	0.0879	9.0900	12.4812	24.6463
0.5938	5.8400	0.0879	8.7600	13.4842	23.7411
0.5455	5.3700	0.0880	8.0550	15.0767	21.8152
0.5080	4.8800	0.0880	7.3200	16.3108	19.8139
0.4611	4.4000	0.0881	6.6000	17.8533	17.8528
0.4158	3.8300	0.0881	5.7450	19.3401	15.5299
0.3950	3.4700	0.0881	5.2050	20.0225	14.0660
0.3605	3.1300	0.0882	4.6950	21.1535	12.6814
0.3225	2.6200	0.0882	3.9300	22.3971	10.6093
0.2965	2.2800	0.0883	3.4200	23.2477	9.2291
0.2648	1.8500	0.0883	2.7750	24.2837	7.4851
0.2385	1.5000	0.0883	2.2500	25.1424	6.0667
0.2991	2.2400	0.0883	3.3600	23.1630	9.0675
0.3408	2.7600	0.0882	4.1400	21.7984	11.1792
0.3962	3.4600	0.0881	5.1900	19.9834	14.0257
0.4698	4.2800	0.0880	6.4200	17.5672	17.3682
0.5280	4.8100	0.0880	7.2150	15.6526	19.5353
0.5800	5.4100	0.0879	8.1150	13.9395	21.9887
0.6480	6.0400	0.0878	9.0600	11.6952	24.5735
0.6865	6.3700	0.0878	9.5550	10.4226	25.9306
0.7545	6.9000	0.0877	10.3500	8.1710	28.1157
0.7545	6.9200	0.0877	10.3800	8.1710	28.1972
0.8210	7.4400	0.0876	11.1600	5.9647	30.3454
0.8930	7.9500	0.0875	11.9250	3.5713	32.4595
0.9531	8.3700	0.0874	12.5550	1.5692	34.2042
0.9932	8.6200	0.0874	12.9300	0.2315	35.2464
1.0000	8.9000	0.0874	13.3500	0.0048	36.3950
1.0000	8.5000	0.0874	12.7500	0.0048	34.7592

R=1150 OUTER CYLINDER VELOCITY = 4.02 CM/SEC

POSIN(IN)	DC VOLTS	THETA	FREQUENCY	POSIN(MM)	VELOCITY(MM/SEC)
1.0000	2.9500	0.0874	14.7500	0.0048	40.2117
0.9510	2.7300	0.0874	13.6500	1.6393	37.1862
0.8940	2.4400	0.0875	12.2000	3.5380	33.2085
0.8380	2.2400	0.0876	11.2000	5.4001	30.4617
0.7690	6.3100	0.0877	9.4650	7.6904	25.7171
0.7030	5.6200	0.0878	8.4300	9.8765	22.8830
0.6500	4.8000	0.0878	7.2000	11.6294	19.5291
0.5770	3.9700	0.0879	5.9550	14.0385	16.1352
0.5140	3.1400	0.0880	4.7100	16.1136	12.7502
0.4610	2.5000	0.0881	3.7500	17.8562	10.1437
0.4080	2.2600	0.0881	3.3900	19.5962	9.1629
0.4890	2.6000	0.0880	3.9000	16.9361	10.5537
0.6600	4.4200	0.0878	6.6300	11.2986	17.9857
0.7660	6.1200	0.0877	9.1800	7.7899	24.9416
0.9390	8.3400	0.0875	12.5100	2.0393	34.0745

R=1670 OUTER CYLINDER VELOCITY = 5.83 CM/SEC

POS'N(IN)	DC VOLTS	THETA	FREQUENCY	POS'N(MM)	VELOCITY(MM/SEC)
1.0000	4.2800	0.0874	21.4000	0.0048	58.3410
0.9715	4.2100	0.0874	21.0500	0.9558	57.3629
0.9470	4.0600	0.0874	20.3000	1.7726	55.2994
0.9202	3.9400	0.0875	19.7000	2.6655	53.6439
0.8870	3.7800	0.0875	18.9000	3.7711	51.4407
0.8070	3.5400	0.0876	17.7000	6.4300	48.1186
0.7615	3.3000	0.0877	16.5000	7.9392	44.8267
0.7126	3.0600	0.0877	15.3000	9.5590	41.5371
0.6471	2.7000	0.0878	13.5000	11.7250	36.6157
0.5905	2.5700	0.0879	12.8500	13.5935	34.8241
0.5411	2.3200	0.0880	11.6000	15.2217	31.4141
0.5040	2.1600	0.0880	10.8000	16.4428	29.2319
0.5040	6.9500	0.0880	10.4250	16.4428	28.2169

0.4690	6.4500	0.0881	9.6750	17.5935	26.1737
0.4322	5.9400	0.0881	8.9100	18.8019	24.0913
0.4030	5.5000	0.0881	8.2500	19.7603	22.2974
0.3775	4.7300	0.0882	7.0950	20.5961	19.1687
0.3295	3.9300	0.0882	5.8950	22.1682	15.9156
0.2895	3.0600	0.0883	4.5900	23.4763	12.3851
0.2495	2.2500	0.0883	3.3750	24.7833	9.1015
0.2165	1.5500	0.0884	2.3250	25.8604	6.2669

R=1800 OUTER CYLINDER VELOCITY = 6.35 CM/SEC

POS'N(IN)	DC VOLTS	THETA	FREQUENCY	POS'N(MM)	VELOCITY(MM/SEC)
1.0000	4.7500	0.0874	23.7500	0.0048	64.7476
1.0000	4.6400	0.0874	23.2000	0.0048	63.2481
0.9778	4.5400	0.0874	22.7000	0.7455	61.8649
0.9465	4.3800	0.0874	21.9000	1.7893	59.6576
0.8970	4.1300	0.0875	20.6500	3.4381	56.2119
0.8531	3.8800	0.0876	19.4000	4.8981	52.7755
0.8110	3.6700	0.0876	18.3500	6.2968	49.8886
0.7605	3.4300	0.0877	17.1500	7.9723	46.5920
0.7185	3.2100	0.0877	16.0500	9.3636	43.5769
0.6716	2.9600	0.0878	14.8000	10.9152	40.1558
0.6020	2.6800	0.0879	13.4000	13.2139	36.3207
0.5670	2.4400	0.0879	12.2000	14.3683	33.0513
0.5670	7.8500	0.0879	11.7750	14.3683	31.8999
0.5245	7.2000	0.0880	10.8000	15.7678	29.2405
0.4605	6.2600	0.0881	9.3900	17.8727	25.3995
0.4030	5.0500	0.0881	7.5750	19.7603	20.4730
0.3478	4.0400	0.0882	6.0600	21.5694	16.3654
0.2985	3.4500	0.0883	5.1750	23.1826	13.9655
0.2720	2.5400	0.0883	3.8100	24.0487	10.2779
0.2430	2.1200	0.0883	3.1800	24.9957	8.5748
0.2330	1.8100	0.0884	2.7150	25.3220	7.3199

R=2500 OUTER CYLINDER VELOCITY = 9.56 CM/SEC

POS'N(IN)	DC VOLTS	THETA	FREQUENCY	POS'N(MM)	VELOCITY(MM/SEC)
1.0000	7.0100	0.0874	35.0500	0.0048	95.5538
0.9650	6.9000	0.0874	34.5000	1.1726	94.0064
0.9400	6.7700	0.0874	33.8500	2.0060	92.2016
0.9070	6.5600	0.0875	32.8000	3.1052	89.2988
0.8750	6.4000	0.0875	32.0000	4.1701	87.0802
0.8450	6.2000	0.0876	31.0000	5.1678	84.3222
0.8050	5.9300	0.0876	29.6500	6.4961	80.6032
0.7680	5.7300	0.0877	28.6500	7.7236	77.8429
0.7310	5.4700	0.0877	27.3500	8.9495	74.2708
0.6930	5.2500	0.0878	26.2500	10.2075	71.2444
0.6480	4.9700	0.0878	24.8500	11.6952	67.0009
0.6020	4.6400	0.0879	23.2000	13.2139	62.8835

0.5540	4.2900	0.0879	21.4500	14.7966	58.0997
0.4980	3.9300	0.0880	19.6500	16.6390	53.1812
0.4570	3.5700	0.0881	17.8500	17.9877	48.2810
0.4130	3.1100	0.0881	15.5500	19.4321	42.0332
0.3590	2.5100	0.0882	12.5500	21.2927	33.8975
0.3590	8.1000	0.0882	12.1500	21.2027	32.8171
0.3200	6.8400	0.0882	10.2600	22.4792	27.6966
0.2860	5.6100	0.0883	8.4150	23.5909	22.7050
0.2690	4.9100	0.0883	7.3650	24.1467	19.8670
0.2340	3.8000	0.0884	5.7000	25.2894	15.3680
0.2070	2.6500	0.0884	3.9750	26.1704	10.7130
0.1900	2.1300	0.0884	3.1950	26.7243	8.6087
0.2800	5.1200	0.0883	7.6800	23.7871	20.7200
0.3320	6.9800	0.0882	10.4700	22.0866	28.2684
0.3640	7.9700	0.0882	11.9550	21.0388	32.2927
0.3640	2.5500	0.0882	12.7500	21.0388	34.4402
0.4340	3.1300	0.0881	15.6500	18.7431	42.3164
0.5210	3.8400	0.0880	19.2000	15.8831	51.9805
0.5950	4.3400	0.0879	21.7000	13.4449	58.8118
0.6670	4.9000	0.0878	24.5000	11.0673	66.4697
0.8110	5.8000	0.0876	29.0000	6.2968	78.8430
0.8900	6.2300	0.0875	31.1500	3.6712	84.7857
1.0000	6.8800	0.0874	34.4000	0.0048	93.7818

R=5186 OUTER CYLINDER VELOCITY = 18.1 CM/SEC

POS'N(IN)	DC VOLTS	THETA	FREQUENCY	POS'N(MM)	VELOCITY(MM/SEC)
1.0000	4.4200	0.0874	66.3000	0.0048	180.7480
0.9812	4.1700	0.0874	62.5500	0.6321	170.4781
0.9491	3.8600	0.0874	57.9000	1.7029	157.7308
0.9115	3.6400	0.0875	54.6000	2.9553	148.6595
0.8655	3.3800	0.0875	50.7000	4.4861	137.9485
0.8230	3.2100	0.0876	48.1499	5.8985	130.9294
0.7760	3.0400	0.0877	45.6000	7.4582	123.9109
0.7344	2.9500	0.0877	44.2500	8.8369	120.1699
0.6964	2.8400	0.0878	42.6000	10.0950	115.6251
0.6632	2.7400	0.0878	41.1000	11.1927	111.5002
0.6632	7.9500	0.0878	39.7500	11.1927	107.8378
0.6281	7.6500	0.0878	38.2500	12.3524	103.7157
0.5946	7.3200	0.0879	36.6000	13.4578	99.1935
0.5448	7.1000	0.0880	35.5000	15.0998	96.1429
0.5045	6.8000	0.0880	34.0000	16.4260	92.0269
0.4625	6.4500	0.0881	32.2500	17.8070	87.2374
0.4116	5.8500	0.0881	29.2500	19.4780	79.0640
0.3520	5.0300	0.0882	25.1500	21.4318	67.9232
0.2955	4.3600	0.0883	21.8000	23.2807	58.8277
0.2260	3.1800	0.0884	15.9000	25.5503	42.8636
0.1862	2.5000	0.0884	12.5000	26.8483	33.6785
0.4390	2.4500	0.0881	36.7500	18.5789	99.3762

R=5338 OUTER CYLINDER VELOCITY = 18.6 CM/SEC

POS'N(IN)	DC VOLTS	THETA	FREQUENCY	POS'N(MM)	VELOCITY(MM/SEC)
1.0000	4.3200	0.0874	64.8000	0.0048	176.6587
0.9800	4.2300	0.0874	63.4500	0.6721	172.9278
0.9568	4.0300	0.0874	60.4500	1.4458	164.6960
0.9245	3.7400	0.0875	56.1000	2.5222	152.7725
0.8915	3.5300	0.0875	52.9500	3.6212	144.1251
0.8594	3.3100	0.0876	49.6500	4.6890	135.0797
0.8255	3.1800	0.0876	47.7000	5.8155	129.7106
0.7905	3.0200	0.0876	45.3000	6.9774	123.1216
0.7385	8.3300	0.0877	41.6500	8.7013	113.1159
0.6921	[illegible]	0.0878	40.2000	10.2373	109.1648
0.6418	7.7100	0.0878	38.5500	11.6997	104.5499
0.5878	7.2500	0.0879	36.2500	13.6825	98.2354
0.5020	6.7600	0.0880	33.8000	16.5086	91.4820
0.4433	6.2500	0.0881	31.2500	18.4379	84.5089
0.4045	5.9800	0.0881	29.9000	19.7110	80.8127

0.3635	5.6000	0.0882	28.0000	21.0552	75.6328
0.3020	5.0000	0.0883	25.0000	23.0681	67.4694
0.2945	4.6000	0.0883	23.0000	23.3131	62.0651
0.2740	4.3000	0.0883	21.5000	23.9833	58.0003
0.2460	3.6500	0.0883	18.2500	24.8977	49.2129
0.2140	3.0000	0.0884	15.0000	25.9420	40.4304

R=5940 OUTER CYLINDER VELOCITY = 20.2 CM/SEC

POS'N(IN)	DC VOLTS	THETA	FREQUENCY	POS'N(MM)	VELOCITY(MM/SEC)
1.0000	3.4400	0.0874	51.6000	0.0048	140.6726
0.9660	3.3200	0.0874	49.8000	1.1389	135.6982
0.9300	3.1400	0.0875	47.1000	2.3393	128.2737
0.8910	2.9000	0.0875	43.5000	3.6376	118.4022
0.8910	8.8400	0.0875	44.2000	3.6376	120.3075
0.8320	8.5600	0.0876	42.8000	5.5995	116.3970
0.7610	7.4800	0.0877	37.4000	7.9554	101.6067
0.6800	6.3000	0.0878	31.5000	10.6373	85.4771
0.6380	5.9300	0.0878	29.6500	12.0256	80.4081
1.0000	3.5400	0.0874	53.1000	0.0048	144.7620
0.9500	3.3700	0.0874	50.5500	1.6726	137.7097
0.9020	3.0500	0.0875	45.7500	3.2717	124.5462
0.8620	2.8200	0.0875	42.3000	4.6025	115.0874
0.8620	8.3700	0.0875	41.8500	4.6025	113.8631
0.8260	7.7900	0.0876	38.9500	5.7986	105.9176
0.7800	7.2800	0.0877	36.4000	7.3255	98.9170
0.7270	6.7900	0.0877	33.9500	9.0824	92.1883
0.6690	6.3600	0.0878	31.8000	11.0012	86.2774
0.6080	5.8900	0.0879	29.4500	13.0158	79.8310
1.0000	4.9300	0.0874	73.9500	0.0048	201.6035
0.9430	4.5500	0.0874	68.2500	1.9060	185.9095
0.8920	4.0300	0.0875	60.4500	3.6046	164.5406
0.8430	3.8000	0.0876	57.0000	5.2339	155.0395
0.7880	3.5200	0.0876	52.8000	7.0601	143.5007
0.7160	3.2000	0.0877	48.0000	9.4464	130.3190

R=6027 OUTER CYLINDER VELOCITY = 21.0 CM/SEC

POS'N(IN)	DC VOLTS	THETA	FREQUENCY	POS'N(MM)	VELOCITY(MM/SEC)
1.0000	5.1300	0.0874	76.9500	0.0048	209.7822
0.9868	5.1000	0.0874	76.5000	0.4448	208.5150
0.9628	4.8000	0.0874	72.0000	1.2460	196.1808
0.9382	4.4000	0.0875	66.0000	2.0657	179.7681
0.9096	4.2000	0.0875	63.0000	3.0186	171.5255
0.8828	4.0500	0.0875	60.7500	3.9108	165.3351
0.8460	3.5500	0.0876	53.2500	5.1342	144.8456
0.8146	3.4000	0.0876	51.0000	6.1772	138.6623
0.7928	3.3000	0.0876	49.5000	6.9010	134.5413
0.7702	3.2000	0.0877	48.0000	7.6506	130.4214
0.7360	3.1000	0.0877	46.5000	8.7838	126.2832
0.7095	2.9000	0.0877	43.5000	9.6613	118.0905
0.6725	2.8000	0.0878	42.0000	10.8854	113.9571
0.6346	2.8000	0.0878	42.0000	12.1377	113.8946
0.5925	2.7000	0.0879	40.5000	13.5271	109.7599
0.5475	2.5500	0.0880	38.2500	15.0104	103.5947
0.5070	2.4000	0.0880	36.0000	16.3440	97.4439
0.4728	2.3000	0.0880	34.5000	17.4686	93.3376
0.4728	7.4000	0.0880	37.0000	17.4686	100.1012

0.4398	7.1000	0.0881	35.5000	18.5526	95.9972
0.3915	6.5000	0.0881	32.5000	20.1373	87.8236
0.3591	5.4000	0.0882	27.0000	21.4937	72.9176
0.3079	4.4000	0.0883	22.0000	22.8750	59.3781
0.2745	3.3000	0.0883	16.5000	23.9665	44.5121
0.2430	2.8300	0.0883	14.0000	24.9957	37.7507
0.2250	1.8000	0.0884	9.0000	26.235	24.2551

R=6055 OUTER CYLINDER VELOCITY = 21.1 CM/SEC

POS'N(IN)	DC VOLTS	THETA	FREQUENCY	POS'N(MM)	VELOCITY(MM/SEC)
0.9920	5.1500	0.0874	77.2500	0.2719	210.5753
0.9775	5.0500	0.0874	75.7500	0.7553	206.4432
0.9545	4.7000	0.0874	70.5000	1.5225	192.0705
0.9197	4.2600	0.0875	63.9000	2.6825	174.0014
0.8806	3.9500	0.0875	59.2500	3.9840	161.2476
0.8481	3.8200	0.0876	57.3000	5.0644	155.8671
0.8015	3.3800	0.0876	50.7000	6.6122	137.8205
0.7713	3.2700	0.0877	49.0500	7.6142	133.2766
0.7287	3.1700	0.0877	47.5500	9.0257	129.1211
0.6749	2.9800	0.0878	44.7000	10.8061	121.2873
0.6220	2.9200	0.0879	43.8000	12.5539	118.7543
0.5628	2.7700	0.0879	41.5500	14.5065	112.5573
0.4965	2.6500	0.0880	39.7500	16.6893	107.5780
0.4390	2.4500	0.0881	36.7500	18.5789	99.3762

R=6200 OUTER CYLINDER VELOCITY = 21.6 CM/SEC

POS'N(IN)	DC VOLTS	THETA	FREQUENCY	POS'N(MM)	VELOCITY(MM/SEC)
1.0000	5.2800	0.0874	79.2000	0.0048	215.9161
0.9860	5.1200	0.0874	76.8000	0.4719	209.3302
0.9660	4.8300	0.0874	72.4500	1.1389	197.4164
0.9330	4.5500	0.0875	68.2500	2.2393	185.8825
0.9020	4.2600	0.0875	63.9000	3.2717	173.9565
0.8620	4.0000	0.0875	60.0000	4.6025	163.2446
0.8230	3.7400	0.0876	56.1000	5.8985	152.5471
0.7830	3.5800	0.0877	53.7000	7.2260	145.9361
0.7420	3.3800	0.0877	50.7000	8.5853	137.7013
0.6990	3.2700	0.0878	49.0500	10.0092	133.1369
0.6430	3.1000	0.0878	46.5000	11.8604	126.1131
0.5730	2.8200	0.0879	42.3000	14.1701	114.6059
0.5220	2.6900	0.0880	40.3500	15.8502	109.2418

R=10820 OUTER CYLINDER VELOCITY = 37.7 CM/SEC

POS'N(IN)	DC VOLTS	THETA	FREQUENCY	POS'N(MM)	VELOCITY(MM/SEC)
1.0000	9.2200	0.0874	138.2999	0.0048	377.0354
0.9660	8.3600	0.0874	125.3999	1.1389	341.6978
0.9170	6.9600	0.0875	104.3999	2.7724	284.2725
0.8820	6.4300	0.0875	96.4499	3.9374	262.4917
0.8440	5.9800	0.0876	89.7000	5.2010	243.9867
0.7930	5.7100	0.0876	85.6499	6.8944	232.7981
0.7400	5.4100	0.0877	81.1500	8.6516	220.3977
0.6810	5.2100	0.0878	78.1499	10.6042	212.0679
0.6420	4.9400	0.0878	74.1000	11.8935	200.9644
0.5890	4.6600	0.0879	69.9000	13.6430	189.4283
0.5330	4.4000	0.0880	66.0000	15.4882	178.7142

0.4960	4.3100	0.0880	64.6500	16.7054	174.9652
0.4490	4.1200	0.0881	61.8000	18.2507	167.1387
0.4020	3.8700	0.0881	58.0500	19.7931	156.8901
0.3470	3.6100	0.0882	54.1500	21.5956	146.2335
0.2990	3.2600	0.0883	48.9000	23.1663	131.9646
0.2520	2.8800	0.0883	43.2000	24.7020	116.5031
0.3380	3.4000	0.0882	51.0000	21.8901	137.7089
0.4110	3.8500	0.0881	57.7500	19.4977	156.0995
0.4840	4.2200	0.0880	63.3000	17.1005	171.2818
0.5630	4.5600	0.0879	68.3999	14.4999	185.2935
0.6180	4.8400	0.0879	72.5999	12.6860	196.8278
0.6980	5.2200	0.0878	78.3000	10.0420	212.5272
0.7590	5.5600	0.0877	83.3999	8.0224	226.5704
0.8460	6.0200	0.0876	90.2999	5.1342	245.6256
0.9240	7.0200	0.0875	105.2999	2.5392	286.7524

R=15870 OUTER CYLINDER VELOCITY = 54.7 CM/SEC

POS'N(IN)	DC VOLTS	THETA	FREQUENCY	POS'N(MM)	VELOCITY(MM/SEC)
1.0000	4.0100	0.0874	60.1499	0.0048	546.6
0.9592	3.2700	0.0874	49.0500	1.3661	445.5
0.9260	3.0400	0.0875	45.6000	2.4722	413.9
0.8765	2.7900	0.0875	41.8500	4.1202	379.6
0.8319	2.6400	0.0876	39.6000	5.6028	359.0
0.7885	2.5500	0.0876	38.2500	7.0438	346.5
0.7885	8.1000	0.0876	121.4999	7.0438	330.2170
0.7231	7.8200	0.0877	117.2999	9.2112	318.5000
0.6468	7.2200	0.0878	108.2999	11.7349	293.7373
0.5682	6.7500	0.0879	101.2500	14.3284	274.3040
0.5160	6.4500	0.0880	96.7500	16.0477	261.9146
0.4679	6.0700	0.0881	91.0499	17.6297	246.3127
0.4251	5.8800	0.0881	88.2000	19.0351	238.4552
0.3696	5.5500	0.0882	83.2500	20.8549	224.8921
0.3204	5.3000	0.0882	79.5000	22.4661	214.6096
0.2712	5.0900	0.0883	76.3499	24.0748	205.9602

END OF FILE

$SIG

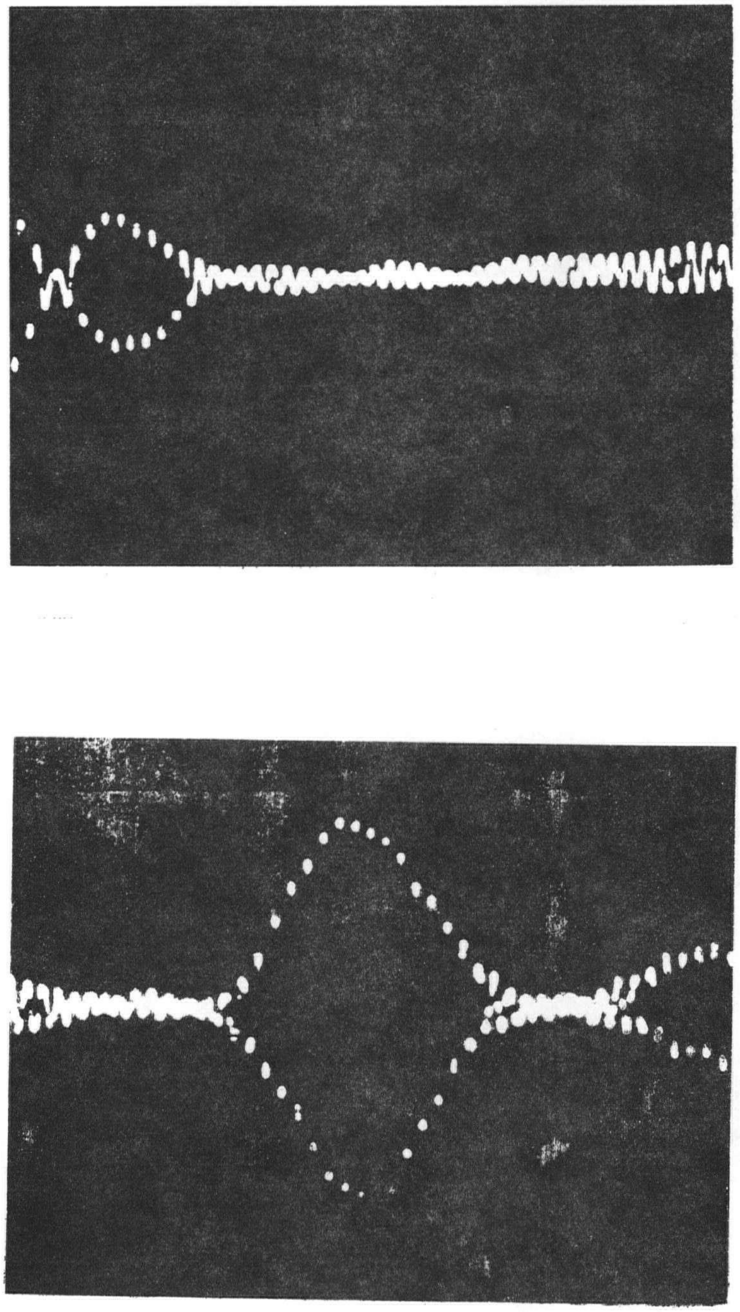

Figure 1.1 Typical LDV signals from particles of approximately uniform size: (a) x = 0.2 msec/cm, y = 5.0 mv/cm; (b) x = 0.2 msec/cm, y = 0.2 mv/cm

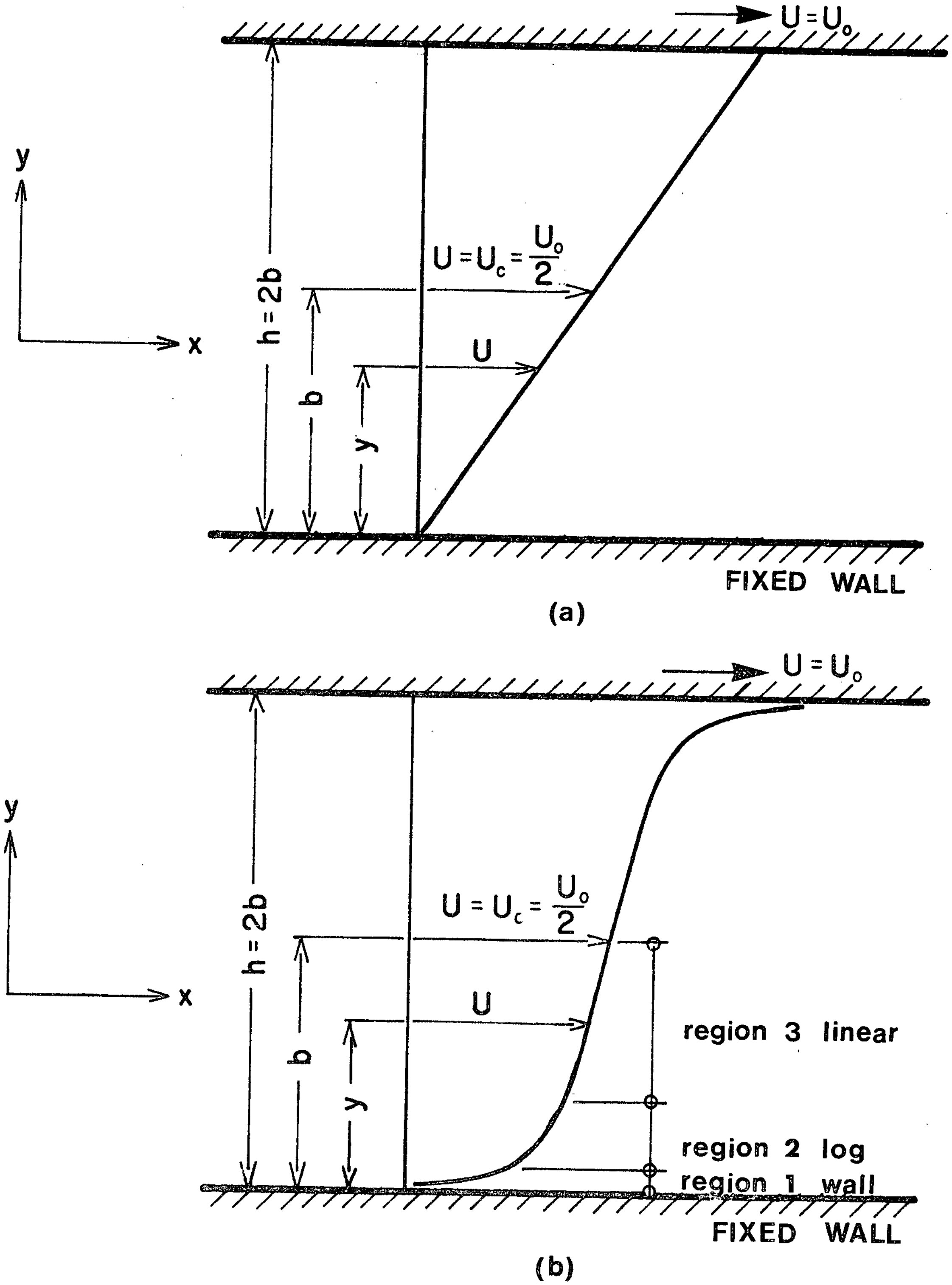

Figure 2.1 Theoretical velocity profiles for plane Couette flow: (a) laminar flow; (b) turbulent flow

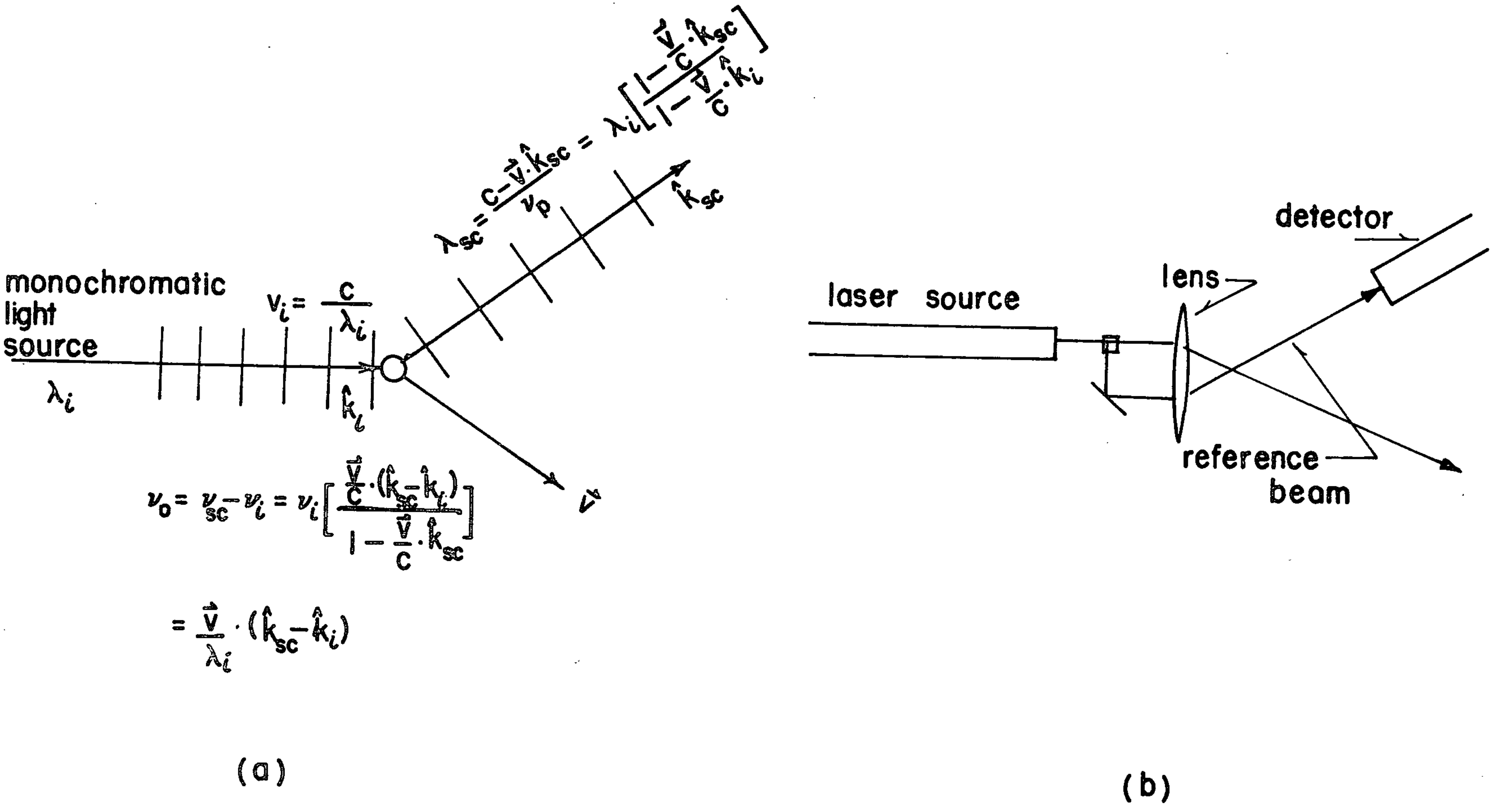

Figure 3.1 Reference beam operation: (a) Schematic of frequency shift; (b) Schematic of optical set up

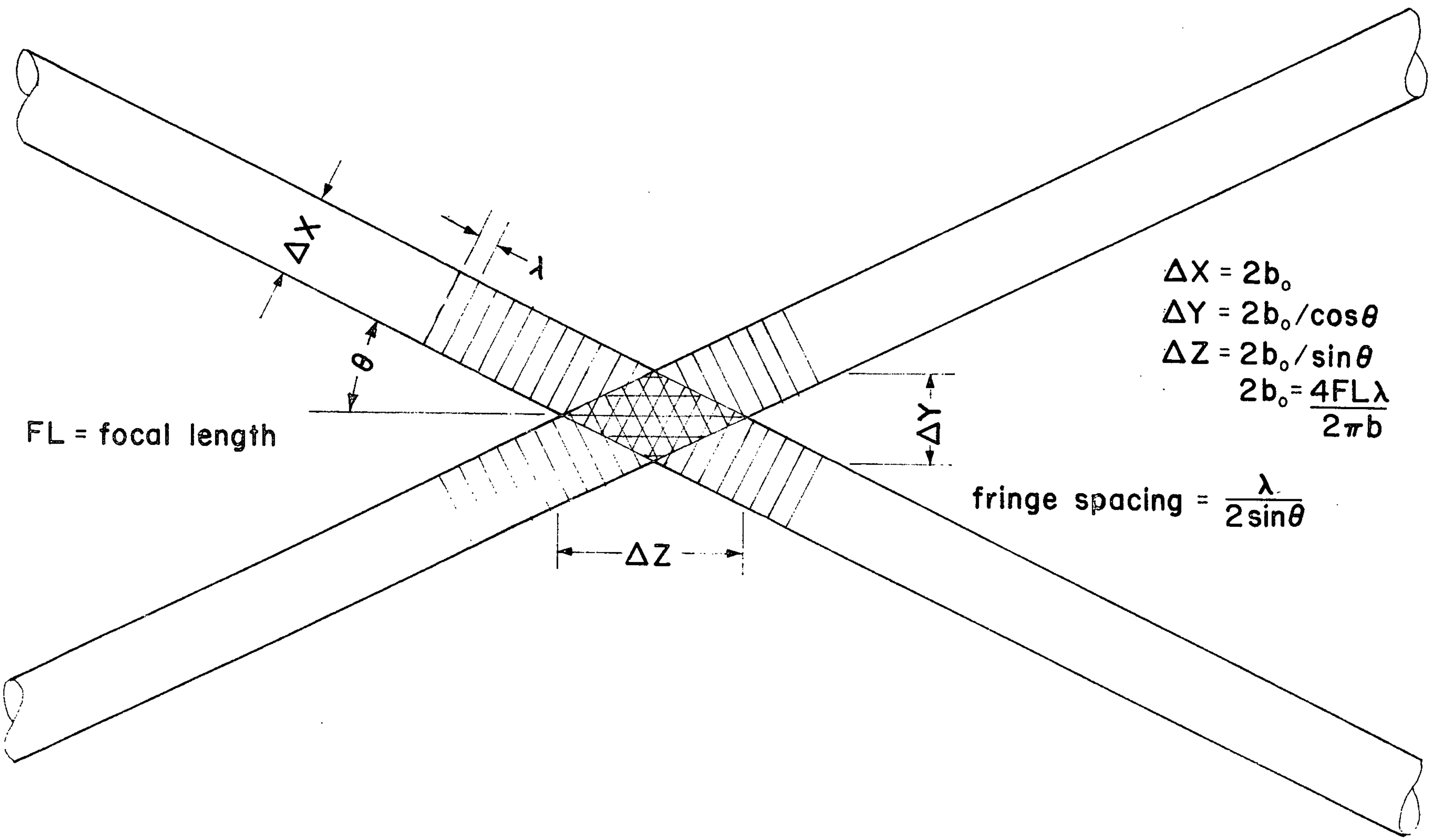

Figure 3.2 Formation of LDV fringe pattern through interference by intersecting laser beams

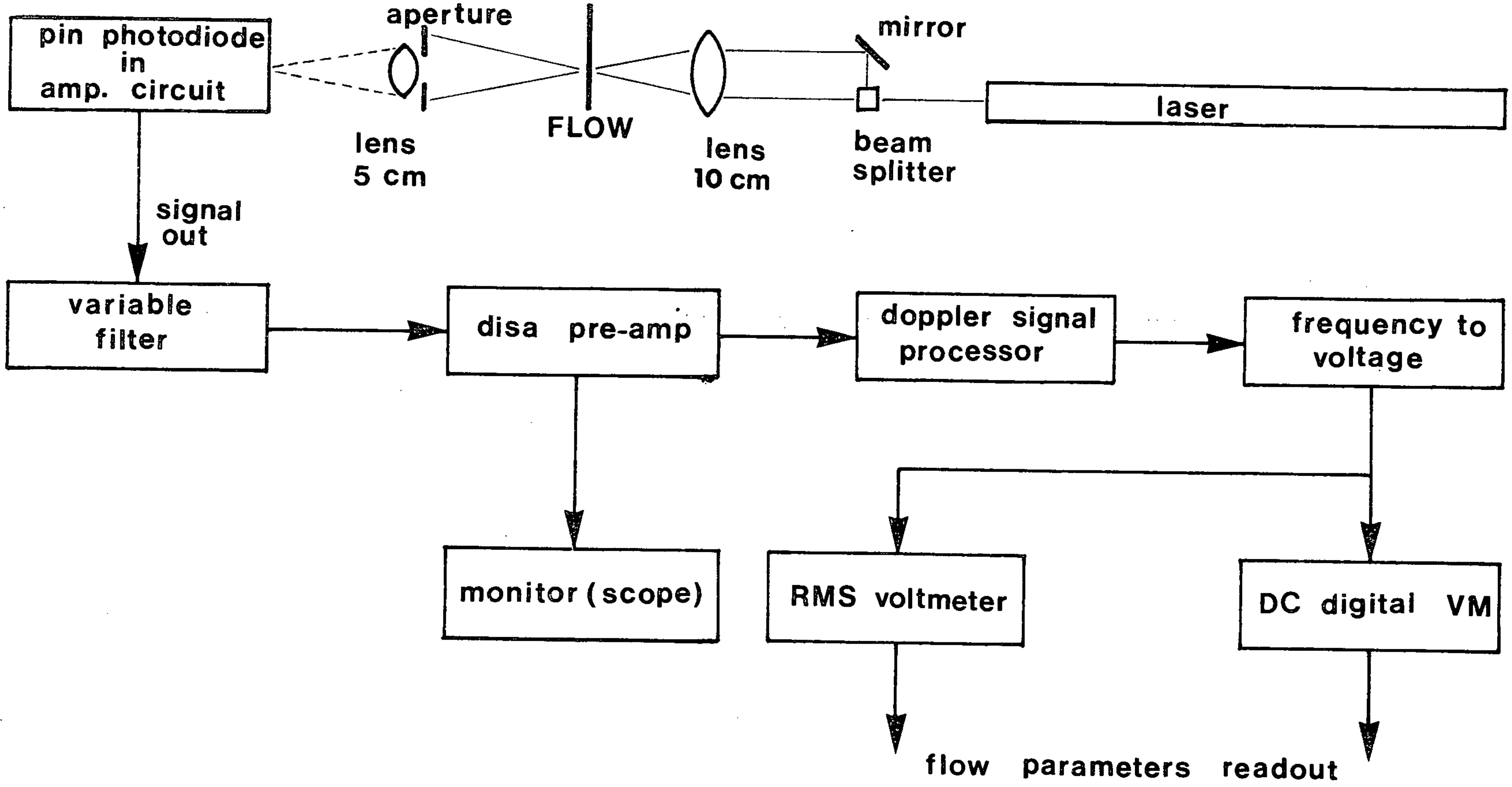

Figure 3.3(a) Schematic illustration of the laser Doppler system used

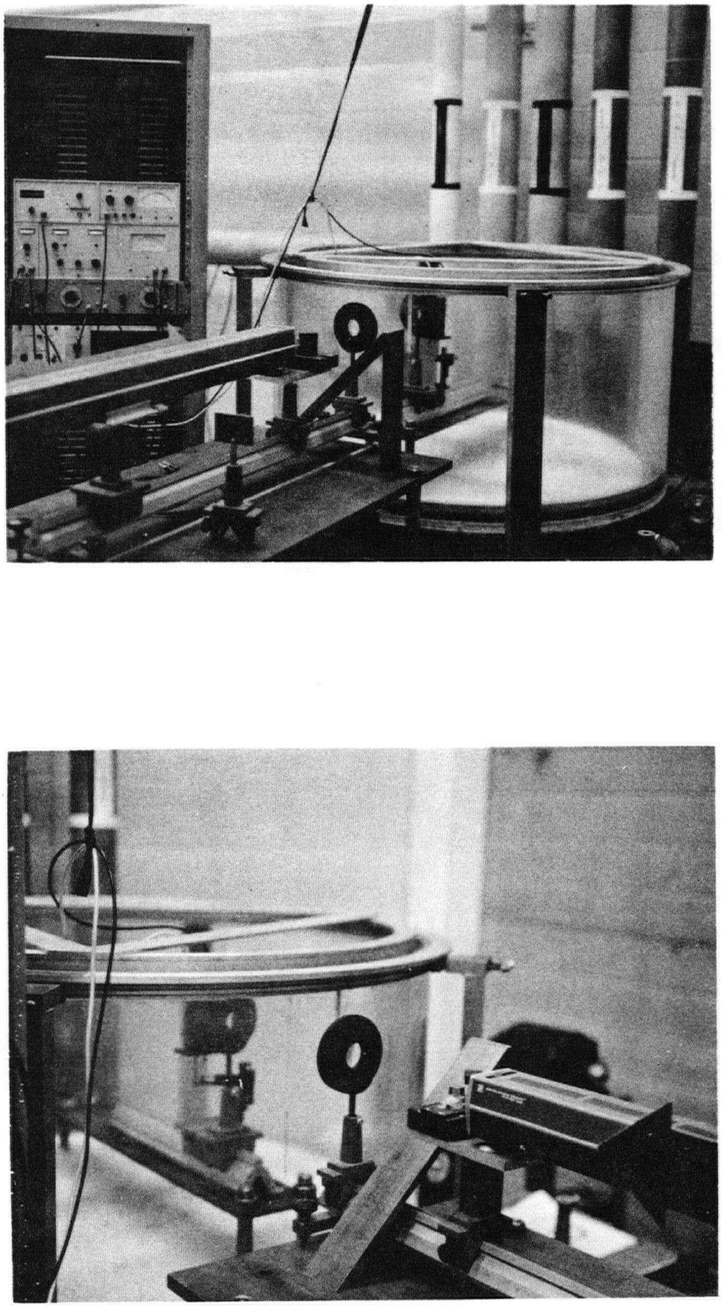

Figure 3.3(b) LDV and Couette flow apparatus

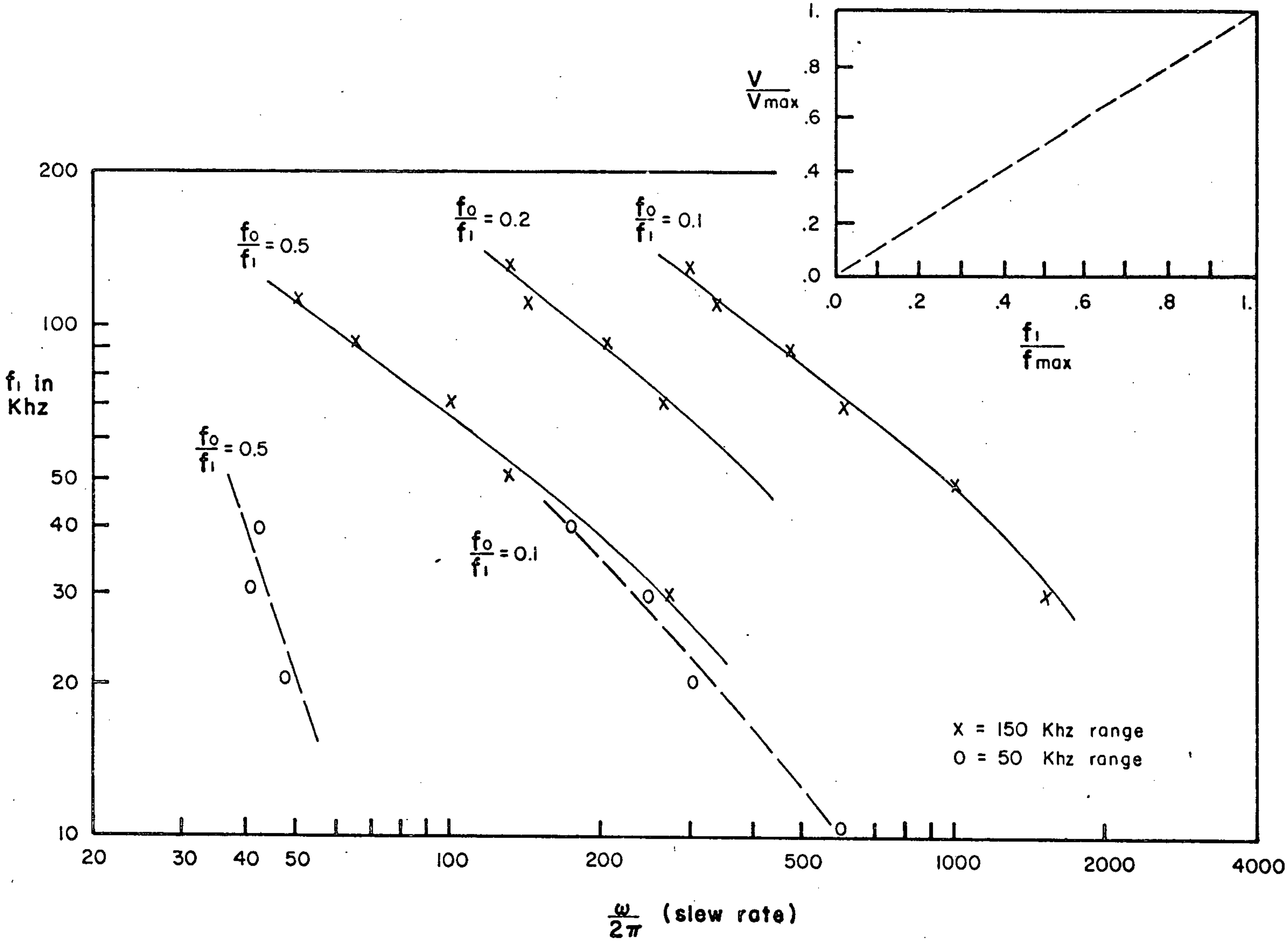

Figure 3.4 Calibration curves for DISA tracker

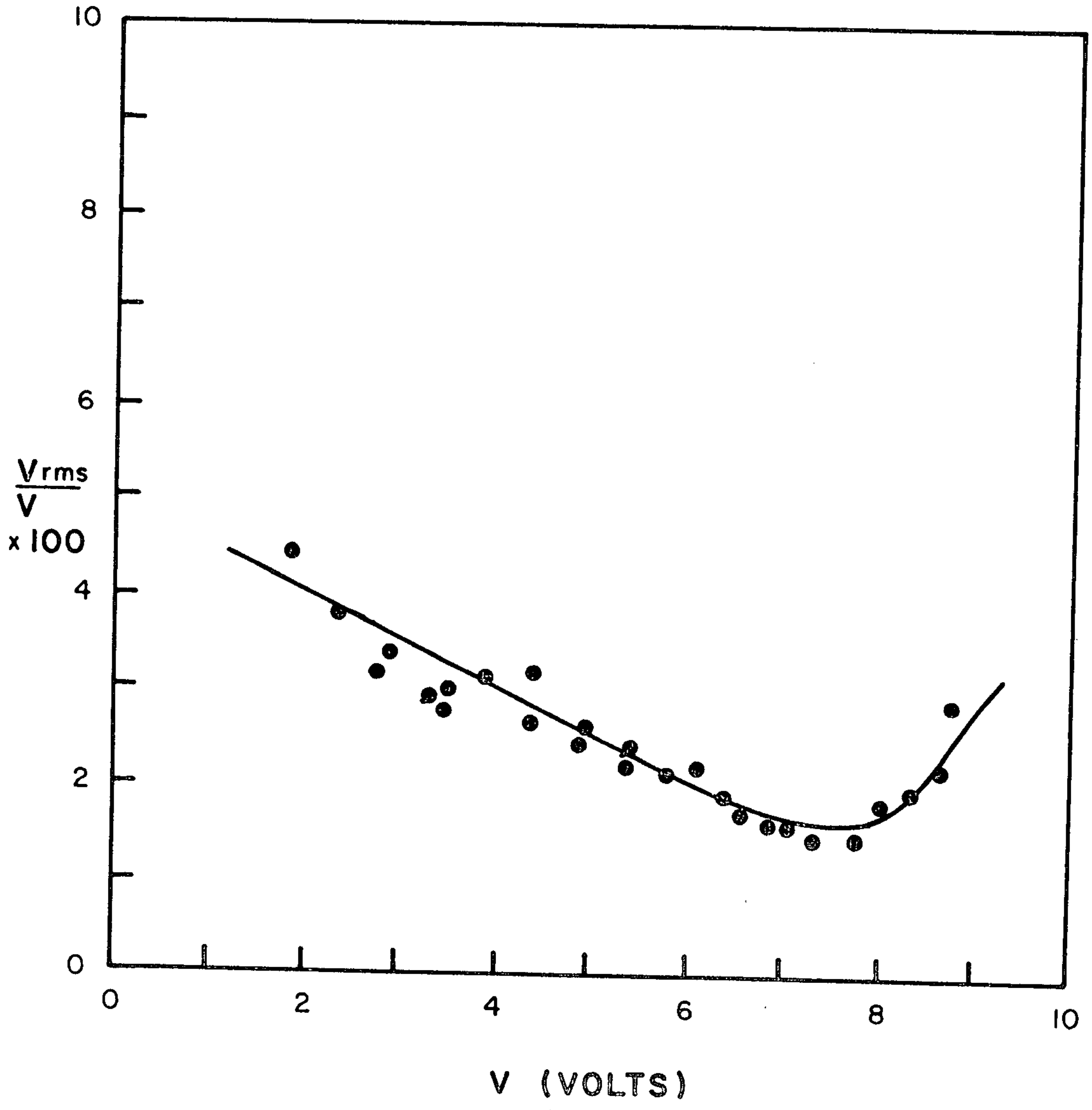

Figure 3.5 Calibration of ambiguous broadening

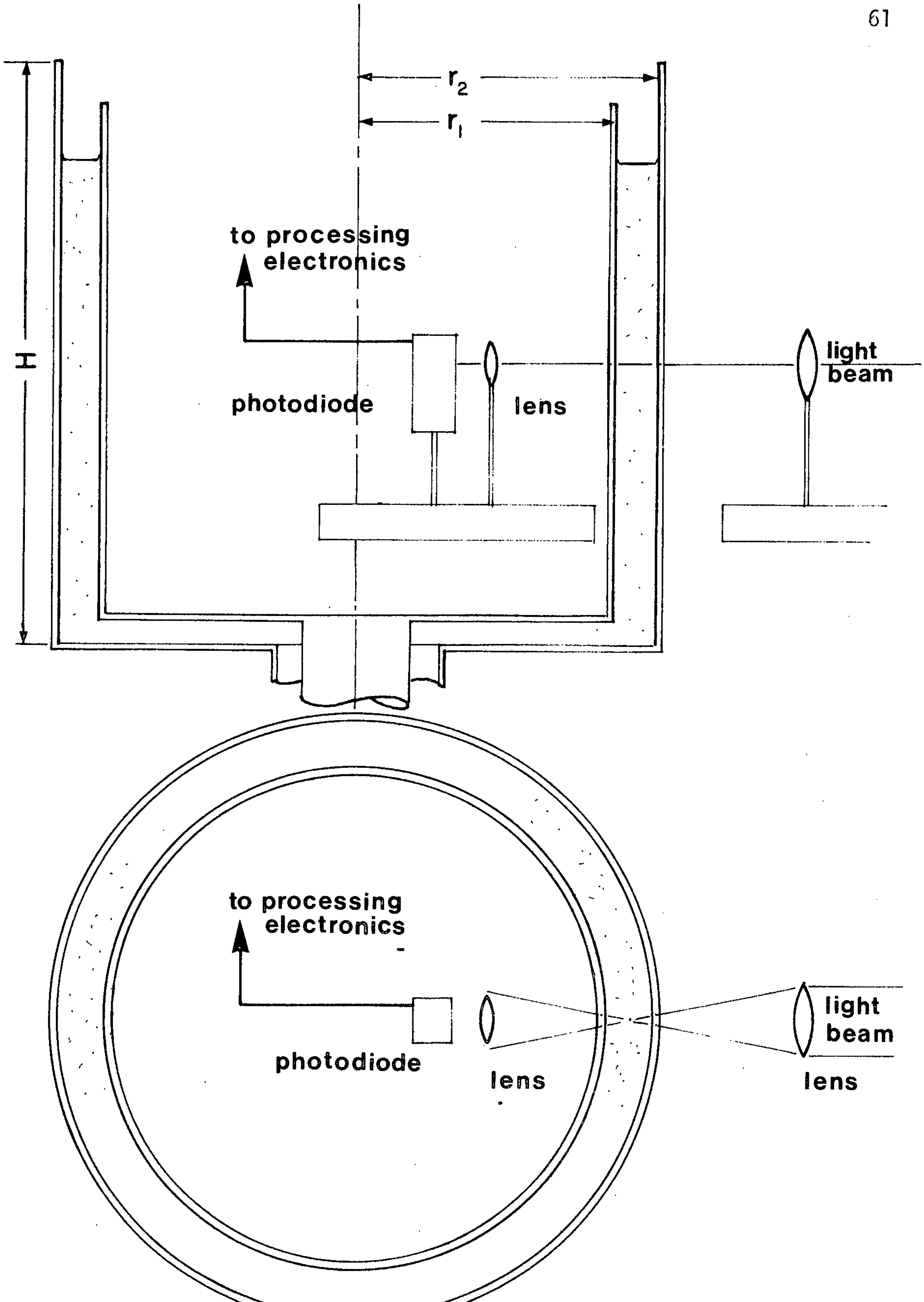

Figure 4.1 Schematic of Couette flow apparatus

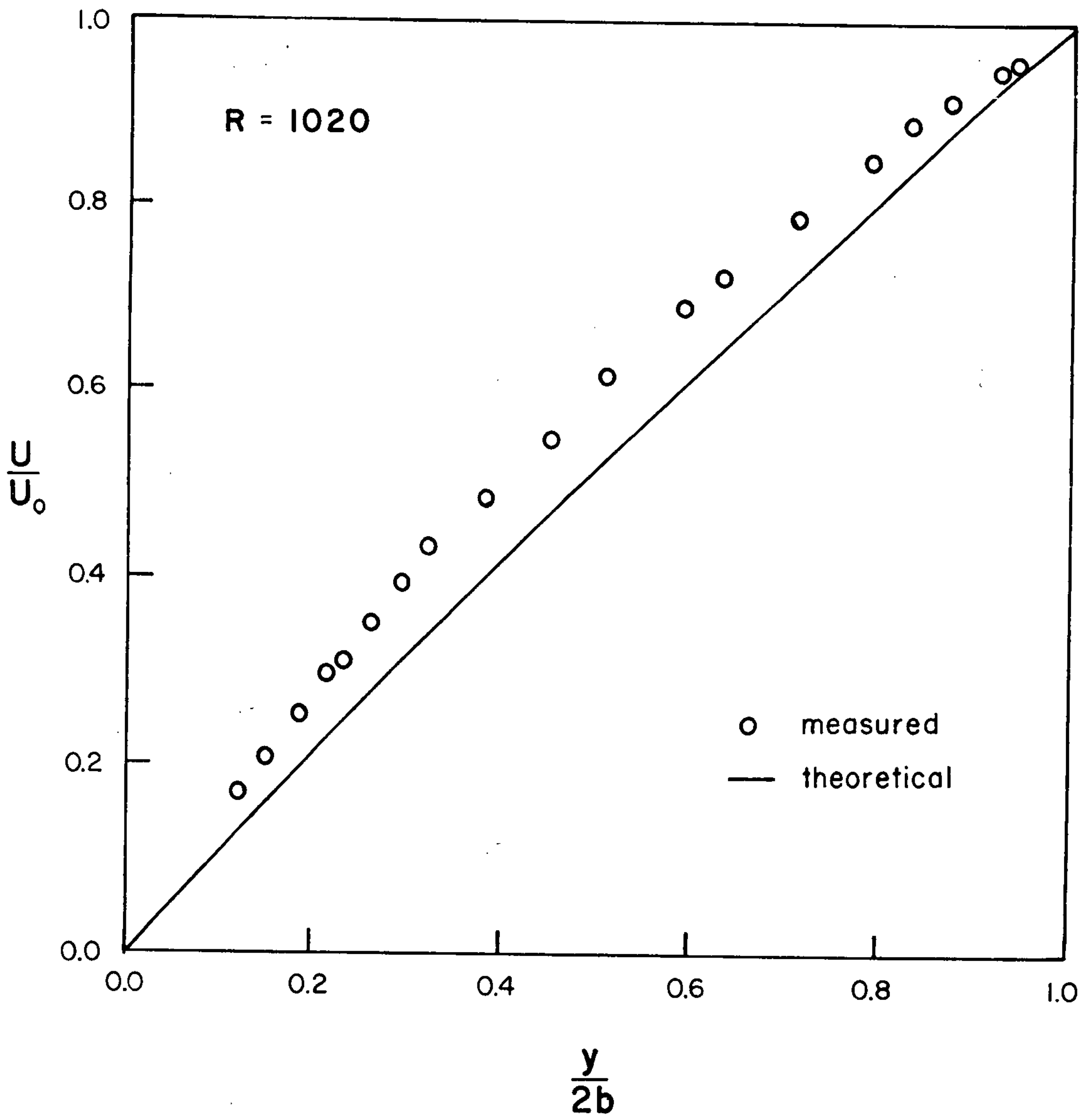

Figure 4.2 Laminar flow profiles. The theoretical flow is for infinite concentric cylinders

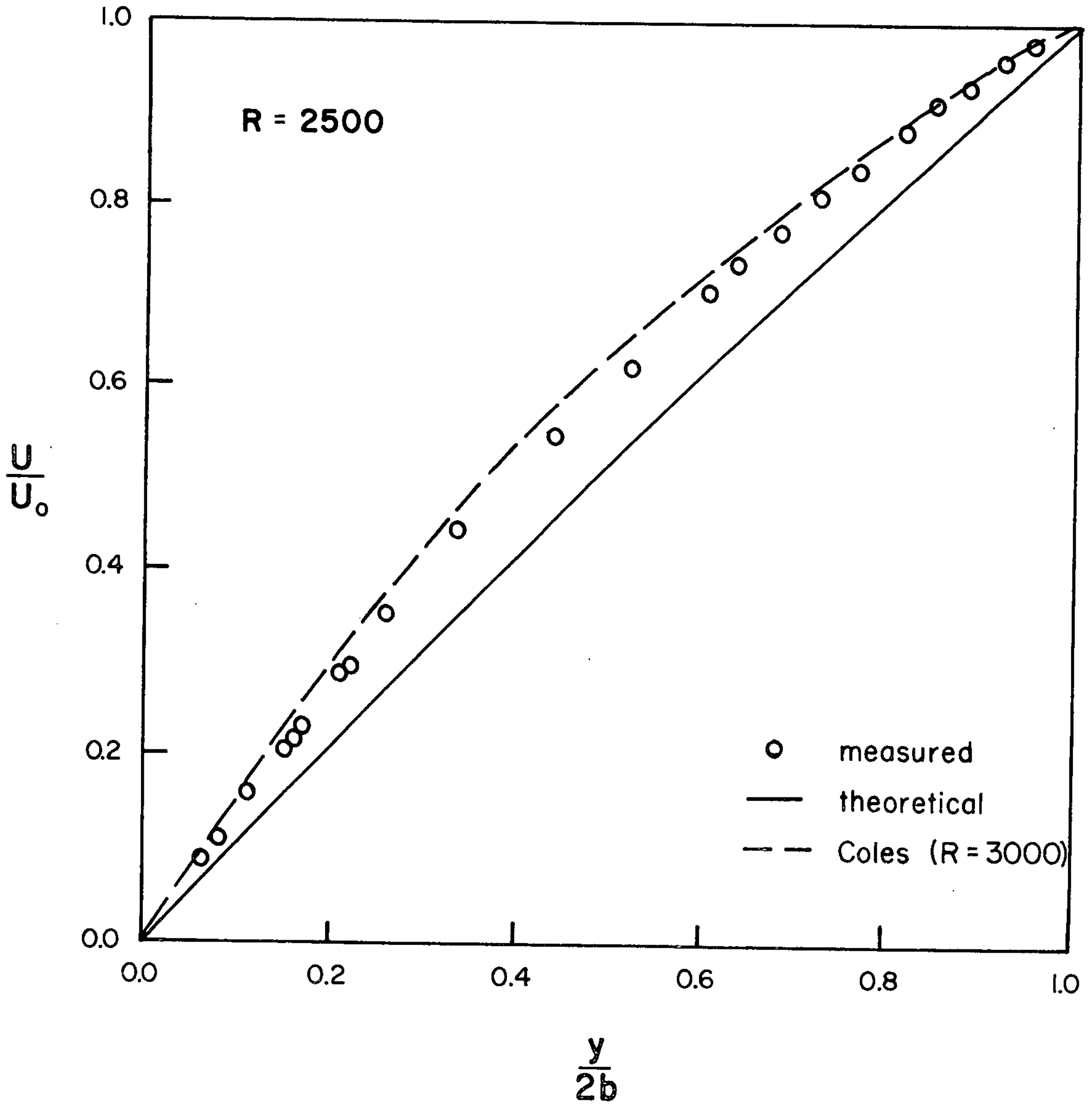

Figure 4.3 Laminar flow profiles. The theoretical flow is for infinite concentric cylinders

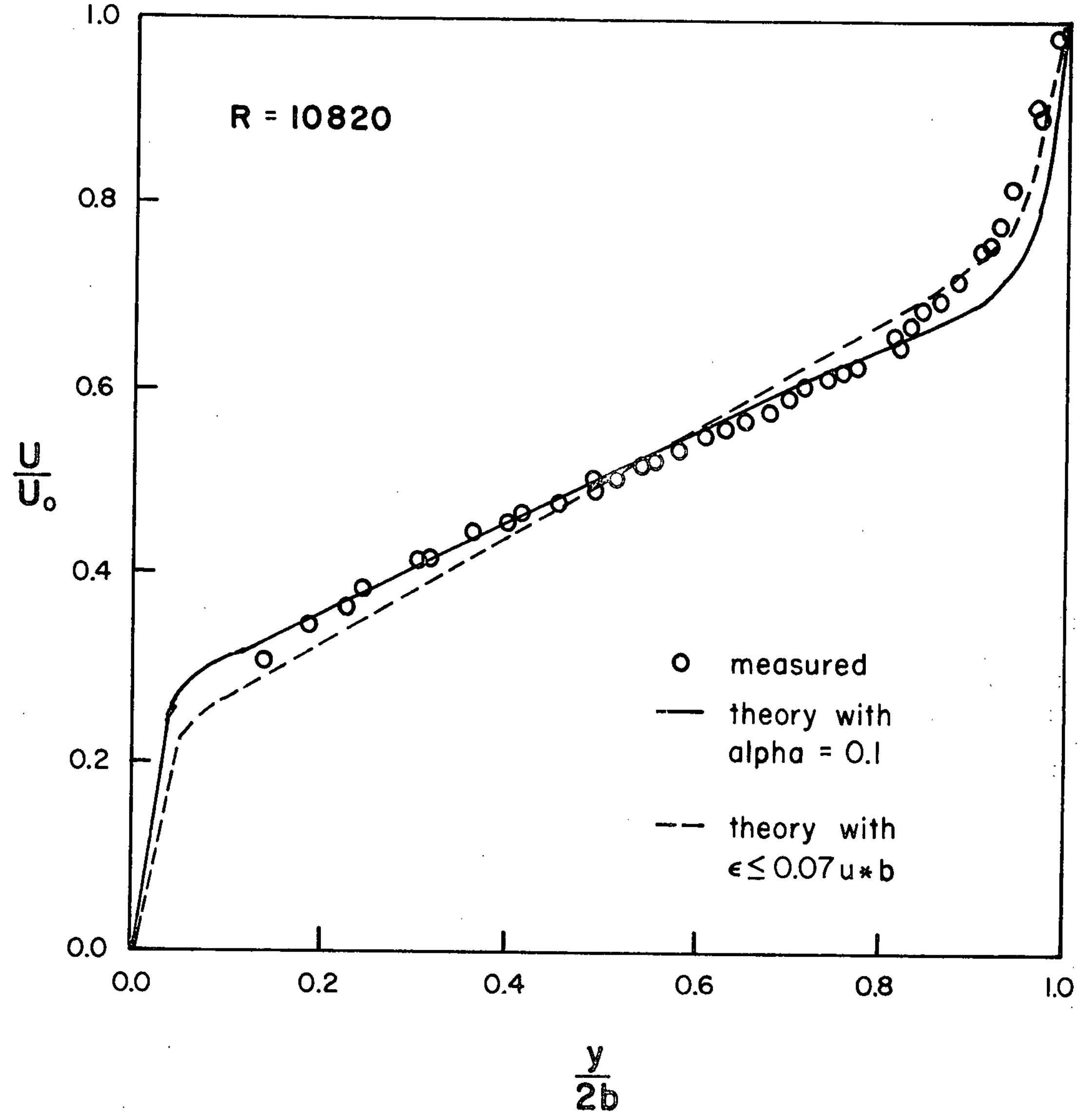

Figure 4.4 Turbulent flow profiles. Theoretical profiles with and without modification proposed by Hinze

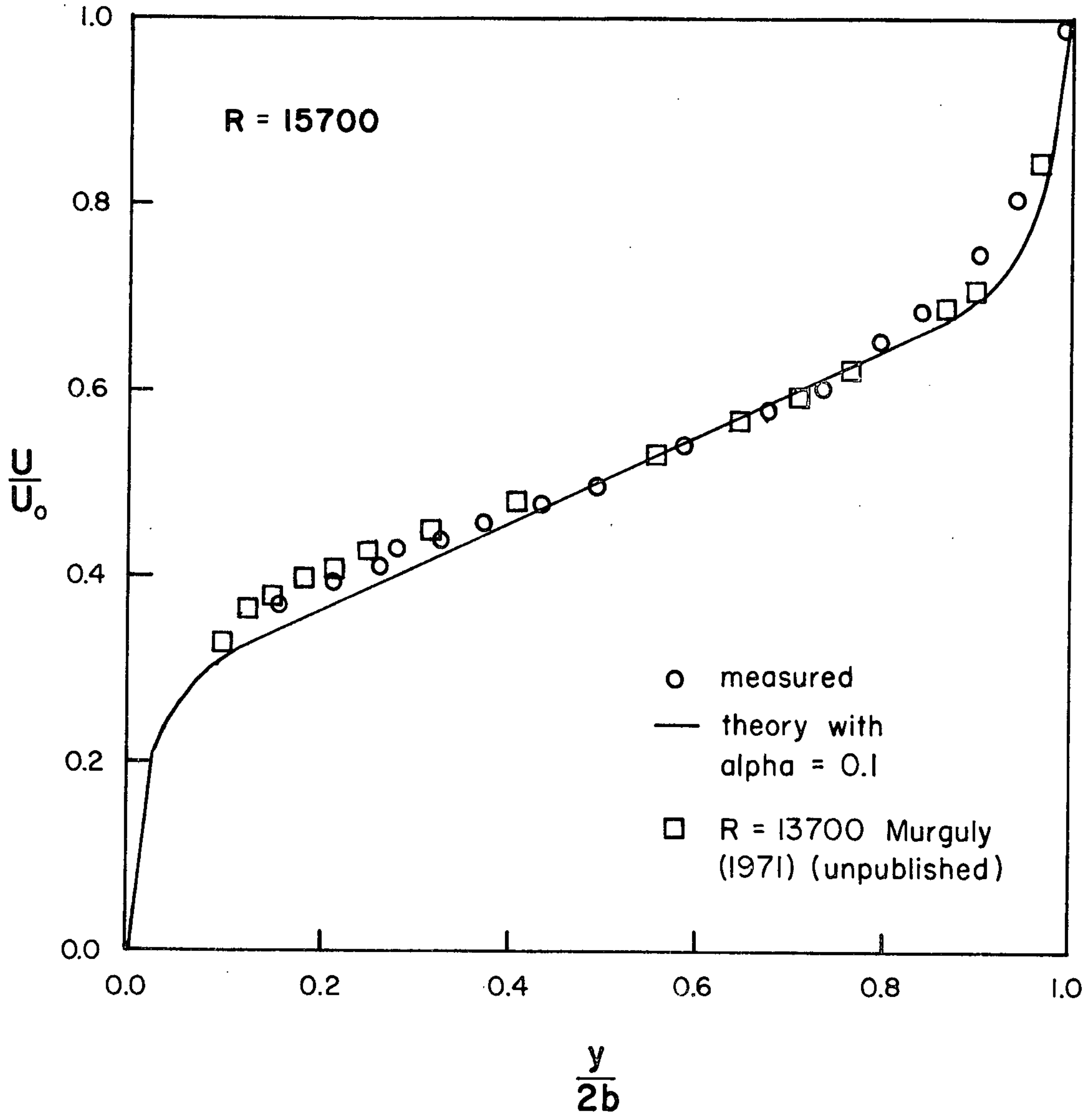

Figure 4.5 Turbulent flow profiles

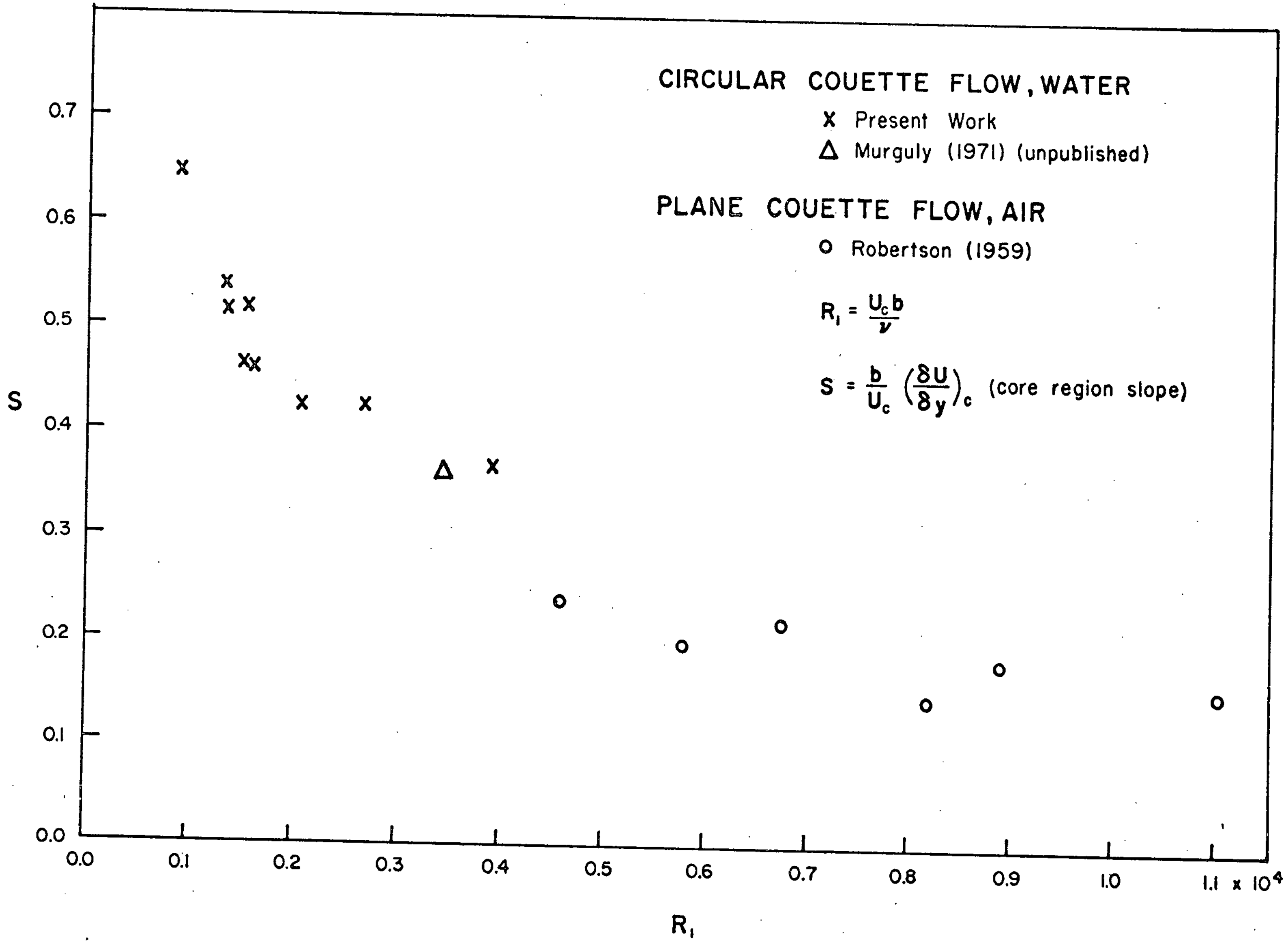

Figure 4.6 Core region slope as a function of Reynolds number

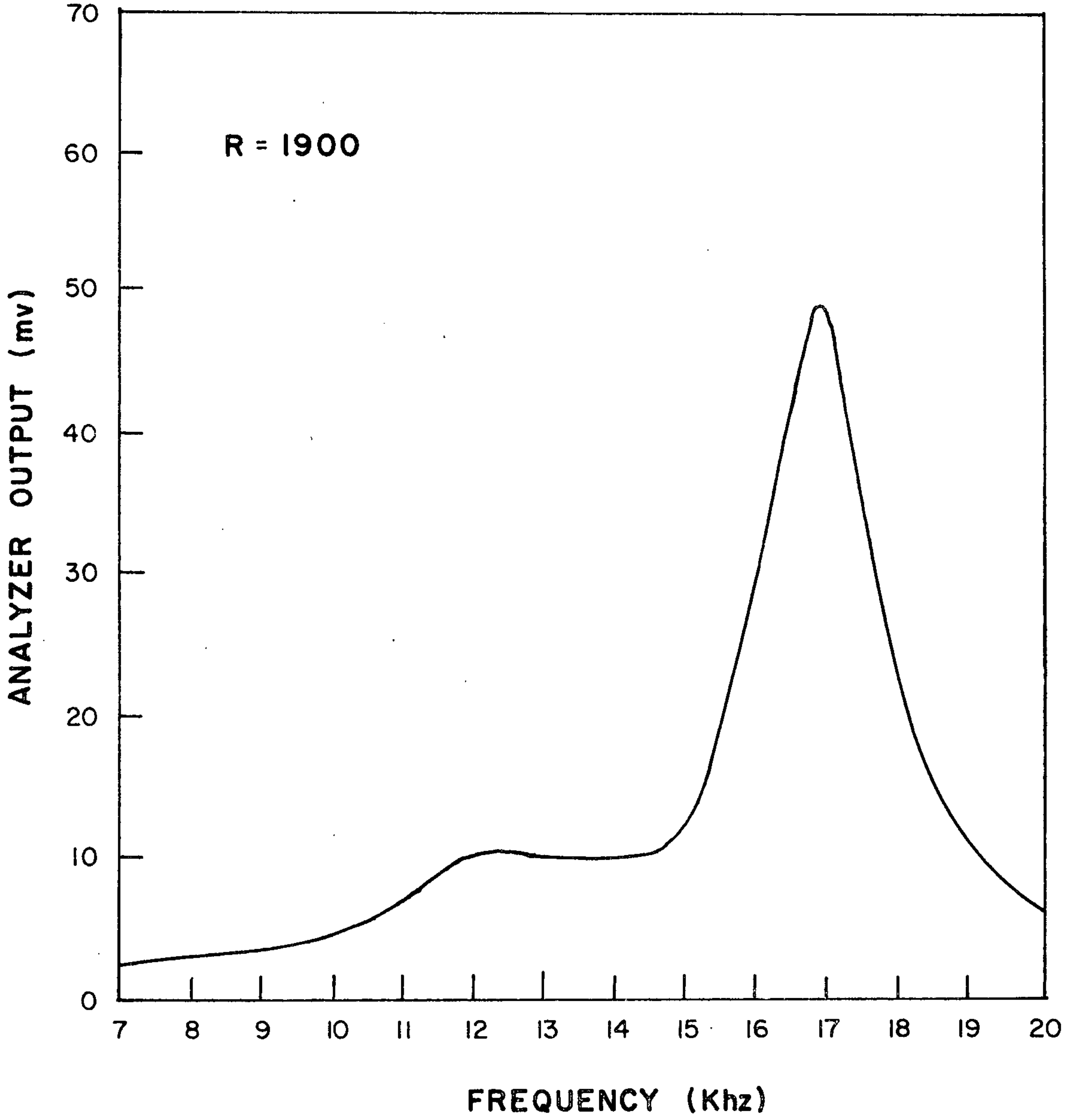

Figure 4.7 Typical laminar flow spectrum. $\bar{U}$ = 4.8 cm/sec

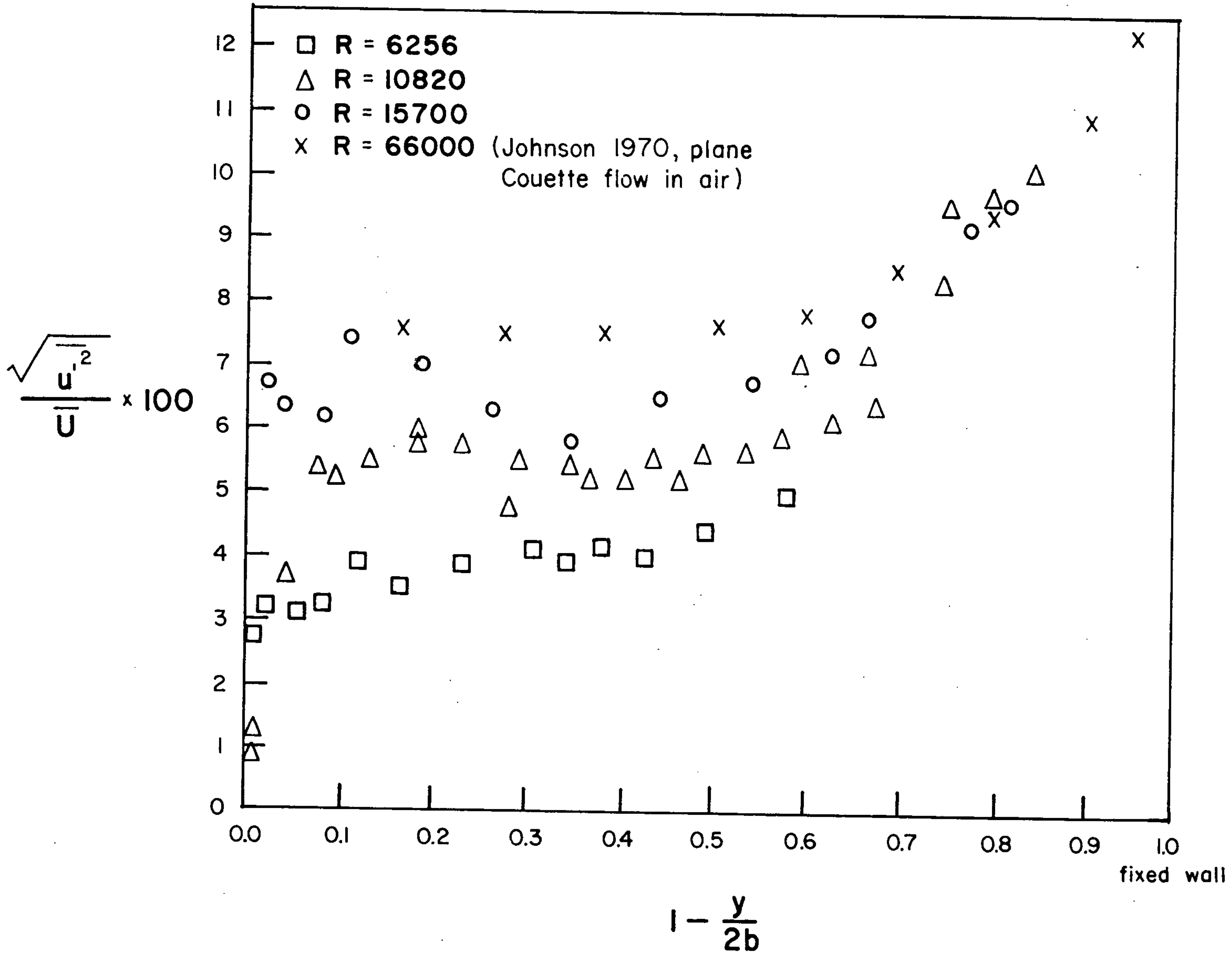

Figure 4.8 $\overline{u'^2}$ turbulence intensities vs normalized position

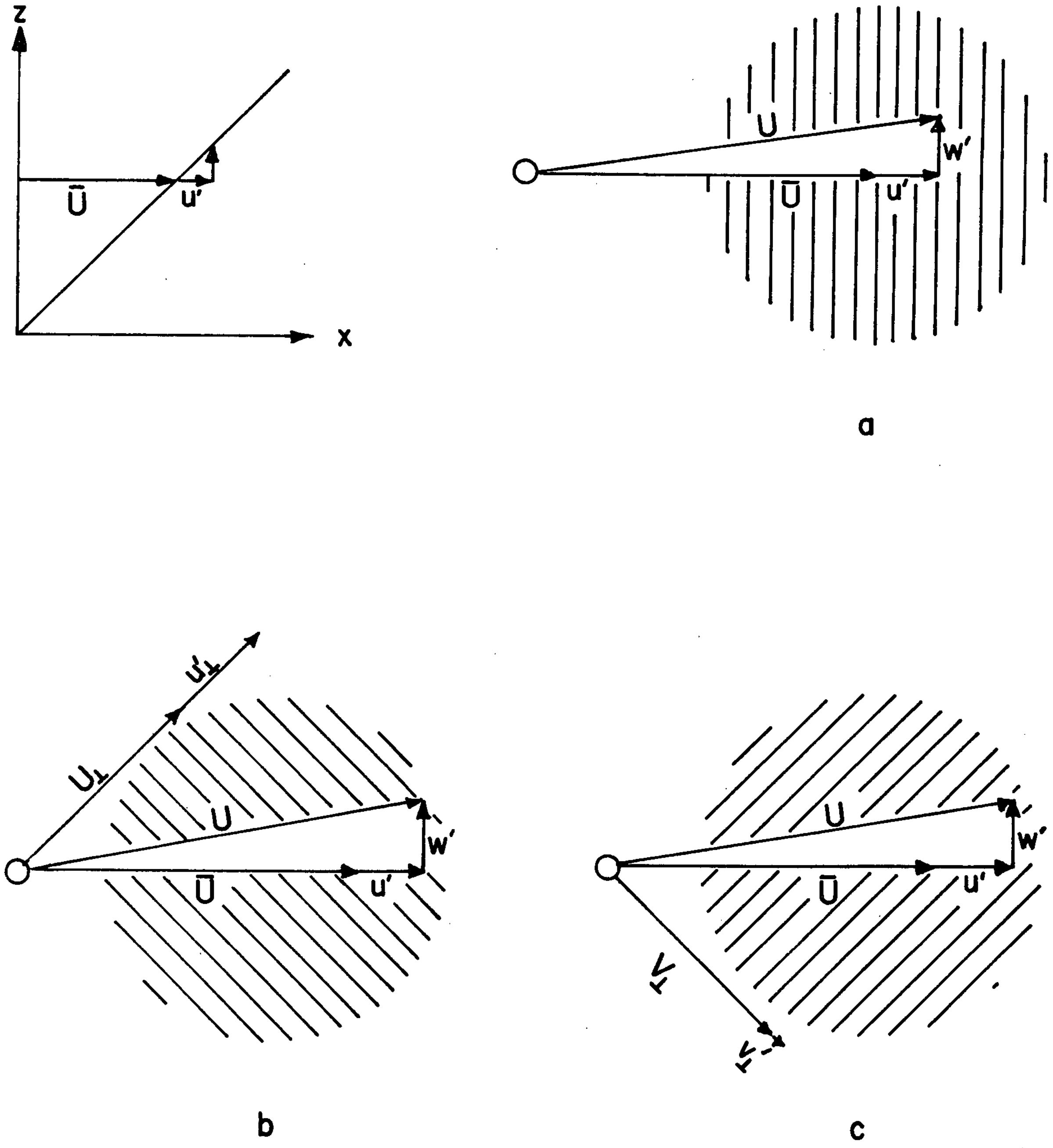

Figure 4.9 Measurement of Reynolds stresses (a) normal fringe pattern; (b) counter clockwise fringe rotation (looking from source; (c) clockwise rotation of fringes

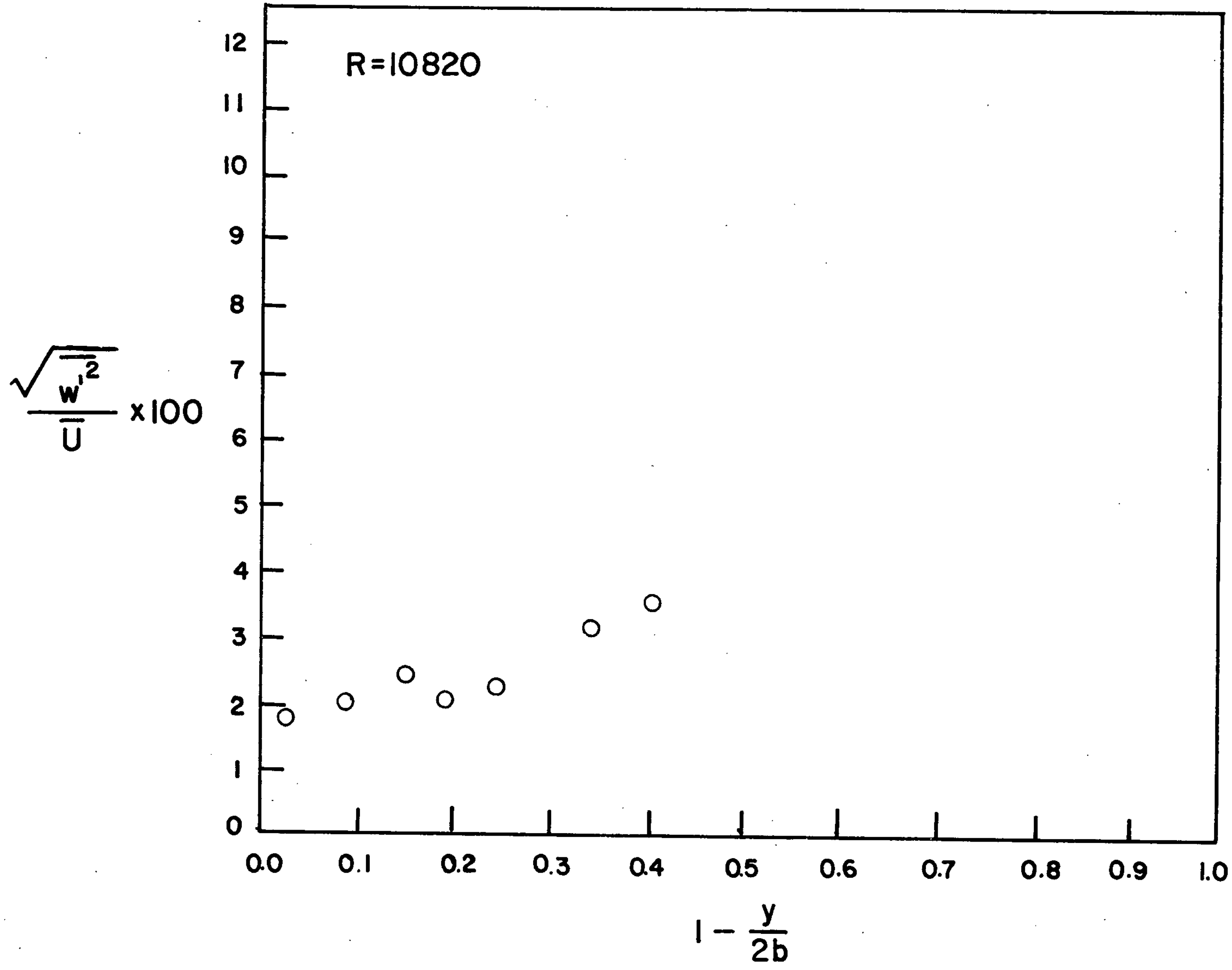

Figure 4.10 $\overline{w'^2}$ turbulence intensities vs normalized position

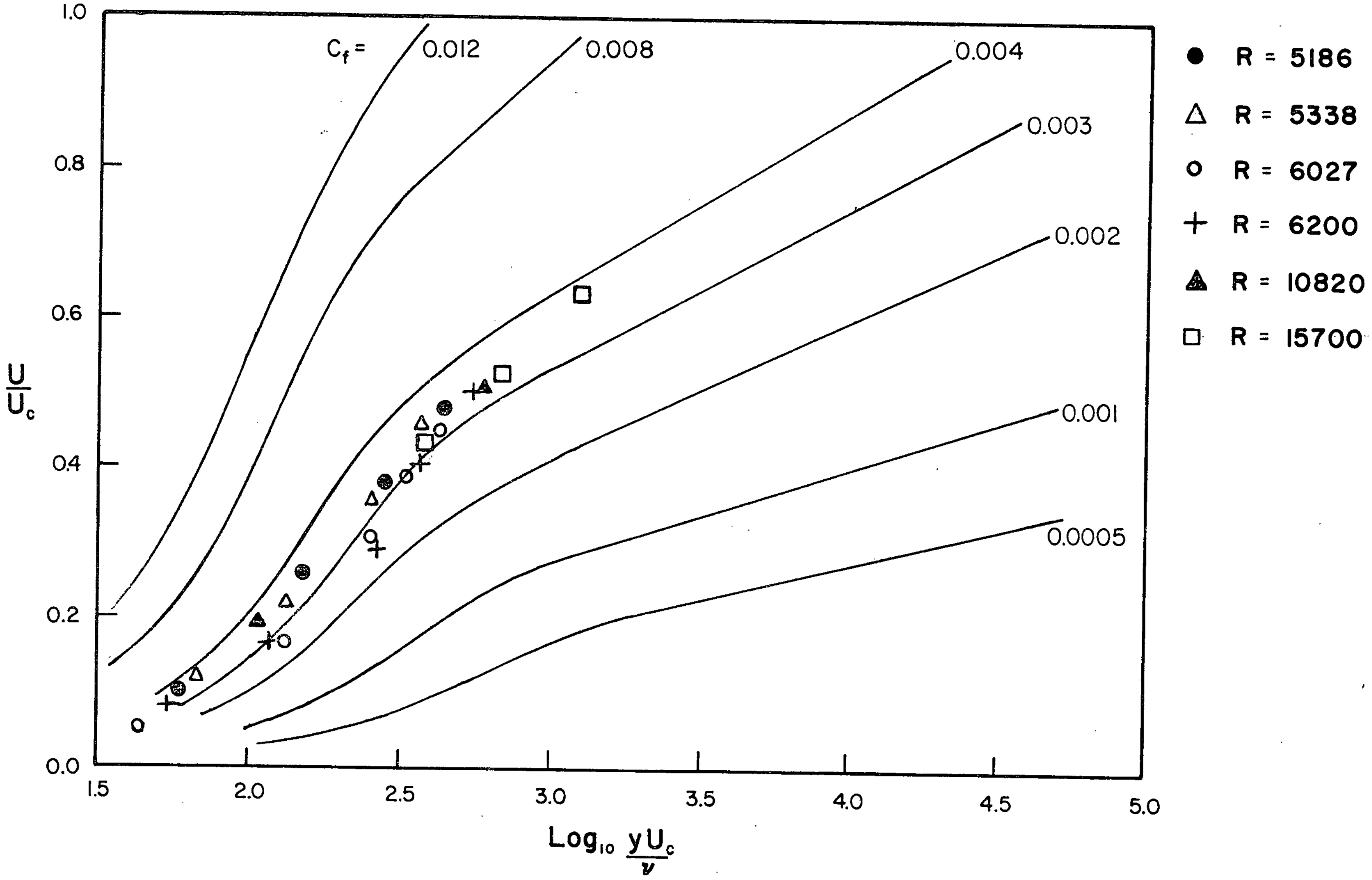

Figure 5.1 Determination of C_f from the Clauser curves

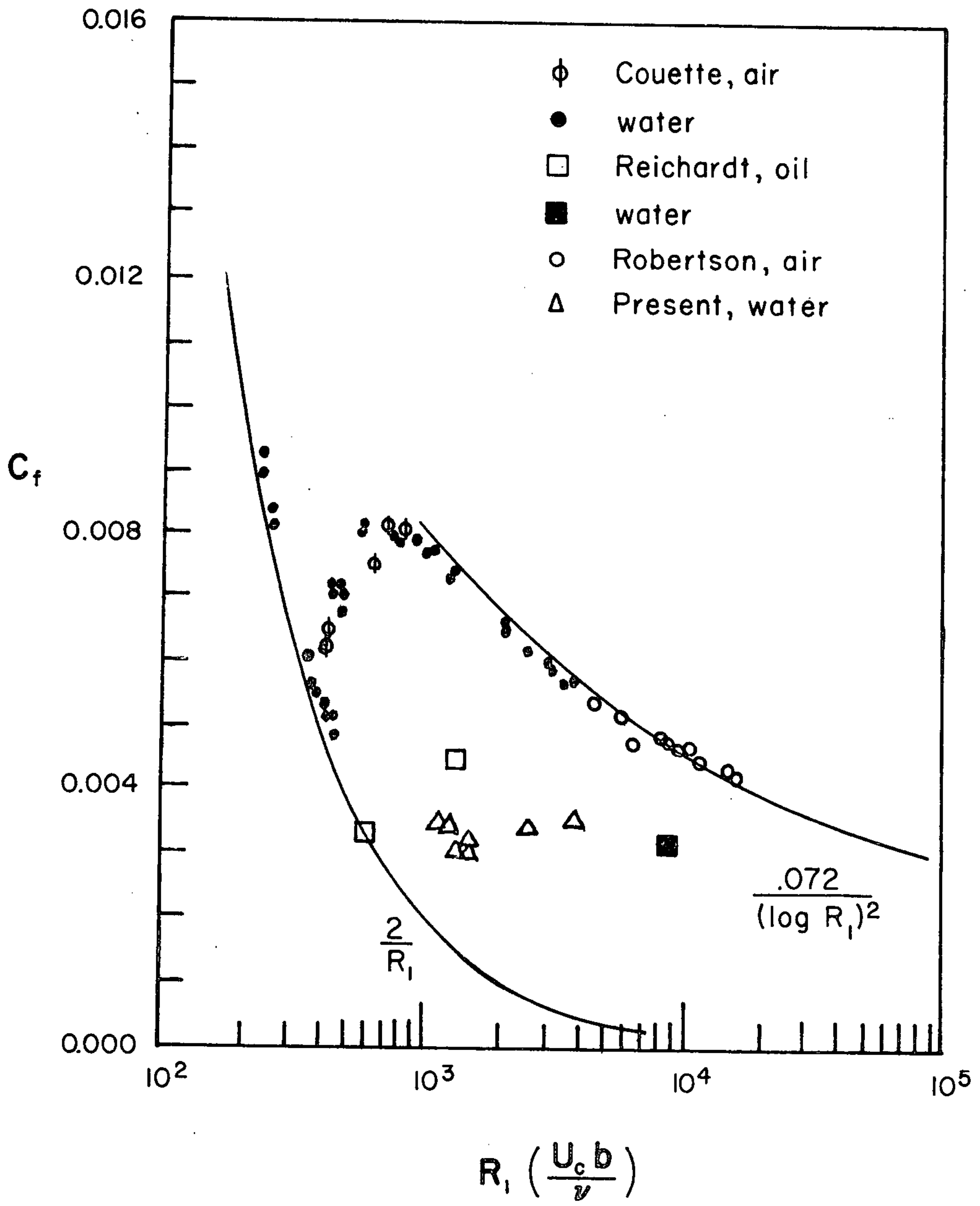

Figure 5.2 Skin friction coefficients vs Reynolds number from various workers

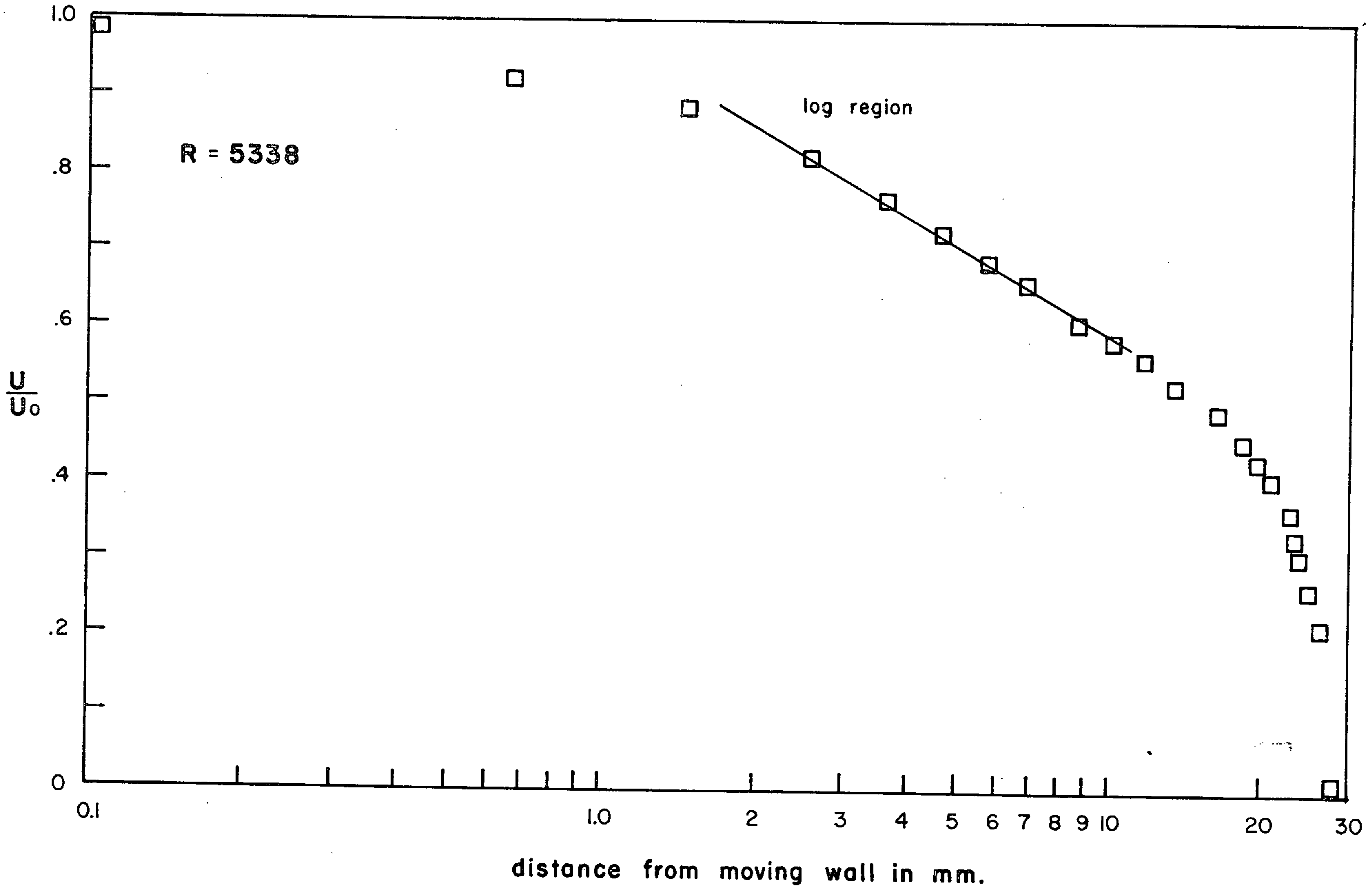

Figure 5.3 Representative semi-log plot showing the logarithmic wall region